

# **Image-Processing Based Gas Hold-Up and Mass Transfer Coefficients Measurements in Bubble Columns**

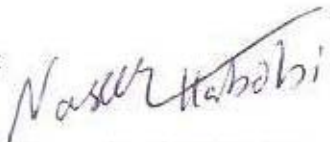
A Thesis  
Submitted to the College of Engineering  
of Nahrain University in Partial Fulfillment  
of the Requirements for the Degree of  
Master of Science  
in  
Chemical Engineering

by  
**Marwa Tariq Rasheed**  
(B.Sc. in Chemical Engineering 2004)

### Certification

I certify that this thesis entitled "Image-Processing Based Gas Hold-Up and Mass Transfer Coefficients Measurements in Bubble Columns", was prepared by "Marwa Tariq Rasheed" under my supervision at Nahrain University/College of Engineering in partial fulfillment of the requirements for the degree of Master of Science in Chemical Engineering.

Signature:



Name: Dr. Naseer A. Al-Habobi  
(Supervisor)

Date: 13 / 2 / 2008

Signature:



Name: Dr. Qasim J. Slaiman  
(Head of Department)

Date: 17 / 2 / 2008

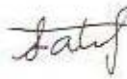
Certificate

We certify, as an examining committee, that we have read this thesis entitled "Image-Processing Based Gas Hold-Up and Mass Transfer Coefficients Measurements in Bubble Columns", and examined the student "Marwa Tariq Rasheed" in its content and found it meets the standard of a thesis for the degree of Master of Science in Chemical Engineering.

Signature: 

Name: Dr. Naseer Habobi  
(Supervisor)

Date: 13 / 2 / 2008

Signature: 

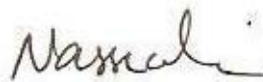
Name: Assist. Prof. Dr. Mohammed N. Latif  
(Member)

Date: 13 / 2 / 2008

Signature: 

Name: Assist. prof. Dr. Malek M. Mohammed  
(Member)

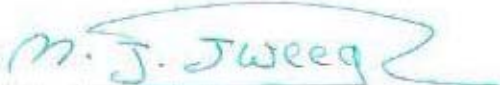
Date: 17 / 2 / 2008

Signature: 

Name: Assist. Prof. Dr. Nasser N. Khamiss  
(Chairman)

Date: 17 / 2 / 2008

Approval of the College of Engineering

Signature: 

Name: prof. Dr. Muhsin J. Jweeg  
(Acting Dean)

Date: 18 / 3 / 2008

## **ABSTRACT**

This thesis suggests a simple system to study, and accordingly design, bubble column reactors. The suggested system focuses on studying two important parameters of the gas-liquid mass transfer operations. These two parameters were the gas hold-up and the interfacial surface area of one bubble.

The system was tested with water as liquid and ambient air as the gas. The images taken were analyzed and manipulated through computer software to produce the required data. Images were manipulated through Adobe Photoshop 7.0 ME and two programs were made with MATLAB to extract the required data from these images.

Three sets of results were obtained for three different diameters of the gas inlet; 0.15, 0.10, and 0.08cm. The results were satisfying and the error in the measurement of interfacial surface area was 0.9%. The error in measuring the gas hold-up ranged from 8% and 15%.

The measured gas hold-up for the gas inlet diameter of 0.15cm ranged between 0.65% and 1.84%. While for the 0.10cm gas inlet diameter, the gas hold-up ranged between 0.96% and 2.13%. And the gas hold-up for the 0.08cm gas inlet diameter lied in the range 1.2% to 2.38%.

The measured average diameters of bubble for the gas inlet diameters of 0.15, 0.1, and 0.08cm were 0.21, 0.15, and 0.1cm, respectively.

This system can be used for the analysis of hydrodynamics of stirred tank models as well as bubble columns. The apparatus used in this system were simple, inexpensive, and acceptably accurate.

## *Table of Contents*

ABSTRACT.....	i
Table of Contents.....	iii
List of Symbols.....	v
List of Abbreviations.....	vi
List of Tables.....	vii
List of Figures.....	viii
Chapter One – Introduction.....	1
1.1 Introduction.....	1
1.2 The Usage of Computers in Experiments.....	2
1.3 Literature Survey.....	4
1.4 Project Aim and Contributions.....	6
1.5 Thesis Layout.....	6
Chapter Two – Gas-Liquid Mass Transfer.....	8
2.1 Introduction to Gas-Liquid Mass Transfer.....	8
2.2 Models.....	11
2.3 Factors Affecting Gas-Liquid Mass Transfer.....	16
2.4 Solubility of Gases in Liquids.....	27
Chapter Three – Methods of Measuring Gas Hold-up.....	35
3.1 Introduction.....	35
3.2 Laser Doppler Anemometry.....	35
3.3 Particle Image Velocimetry.....	37
3.4 3D Modeling of Mass Transfer.....	39
3.5 Choosing the Experimental Technique.....	40
Chapter Four – Implementation and Results.....	45
4.1 Introduction.....	45

4.2 Apparatus Used.....	45
4.3 Experimental Procedure.....	48
4.4 Computational Procedure.....	48
4.5 Simplifying Assumptions.....	52
4.6 Results.....	52
4.7 Discussions.....	63
Chapter Five – Conclusions and Future Work.....	70
5.1 Conclusions.....	70
5.2 Suggestions for Future Work.....	71
References.....	72
Appendix A -- The Specifications of the Camera Used in the Experiment.....	A-1
Appendix B -- Matlab Program to Calculate the Percentage of Bubbles in the Liquid.....	B-1
Appendix C -- Matlab Program to Calculate the Interfacial Surface Area of One Bubble.....	C-1

## List of Symbols

$\delta$	Thickness of the interface (m)
$\Delta C$	Concentration driving force (mol/m <sup>3</sup> )
$\Delta G^{\circ}$	Standard chemical free energy of the reaction (J)
$\Delta x$	Fringe spacing (m)
$\varepsilon$	Gas hold-up (%)
$\theta$	Contact time (s)
$\mu_{aq}^{\circ}$	Aqueous standard molar chemical potentials of oxygen (J/mol)
$\mu_g^{\circ}$	Gaseous standard molar chemical potentials of oxygen (J/mol)
$a$	Gas-liquid interfacial area $A$ per unit volume of fluid $V$ (m <sup>2</sup> /m <sup>3</sup> )
$A$	Absorbed gas (-)
$C$	Concentration of absorbed gas $A$ (mol/cm <sup>3</sup> )
$C_G$	Gas concentration (mol/m <sup>3</sup> )
$C_i$	Concentration of ion $i$ in the solution (mol/cm <sup>3</sup> )
$C_L$	Liquid concentration (mol/m <sup>3</sup> )
$d_s$	Bubble diameter (cm)
$D$	Diffusion coefficient of gas $A$ (m <sup>2</sup> /s)
$E$	Angular coefficient in the saturation curve (-)
$f_p$	Measured frequency of the fringe pattern (fringe/m)
$h_i$	Ion-specific parameter (m <sup>3</sup> /kmol)
$H_0$	Dimensionless representation of Henry's law constant in partial oxygen pressure $P$ at 1 atm
$J_A$	Molecular diffusion (mol/m <sup>2</sup> s)
$k_G$	Gas mass transfer coefficient (m/s)
$k_L$	Liquid mass transfer coefficient (m/s)
$k_L a$	Volumetric liquid mass transfer coefficient (1/s)
$K$	Mass transfer coefficient (m/s)
$M$	Magnification of the camera (-)
$N$	Mass transfer rate (mol/m <sup>3</sup> s)
$P$	Pressure (atm)
$R$	Consumption of gas $A$ in reaction when present (m <sup>3</sup> )
$t$	Time (s)
$v_G$	Gas superficial flow rate (m/s)
$v_L$	Liquid velocity (m/s)
$V_s$	Liquid velocity (m/s)

## *List of Abbreviations*

CFD	Computational Fluid Dynamics
FT	Front-Tracking
LDA	Laser Doppler Anemometry
PIV	Particle Image Velocimetry
PTV	Particle Tracking Velocimetry
STP	Standard temperature and pressure (1 atm and 0 Deg C)

## List of Tables

<b>Table No.</b>	<b>Table Title</b>	<b>Page</b>
2.1	Collected data of the Film, Penetration and Surface removal models	15
2.2	Coefficients A, B and C used for calculating Henry's constant	30
4.1	Measured Gas Hold-up for Different Gas Inlet Diameters	55
4.2	Specific Gas-Liquid Interface Area for Different Diameters of Gas Inlet	57
4.3	Thickness of Interface and Interface Area of Bubbles for Different Gas Inlet Diameters	60
4.4	$k_L$ values for Different Gas Inlet Diameters	60
4.5	$k_L$ , $a$ , and $k_L a$ values for different Gas Inlet Diameters	62
4.6	Comparison of Manually Obtained Results and Results of Program 2	66

## List of Figures

Figure No.	Figure Title	Page
1.1	Using a Computer in Obtaining Data from Bubble Column	3
2.1	Schematic presentation of the gas-liquid interface, concentrations and the mass transfer coefficients $K$ , $k_L$ and $k_G$	10
2.2	Concentration change in film model	12
2.3	Relationship Between the Various Factors Affecting the Mass Transfer Rates in a Gas-Liquid Reactor	16
2.4	Calculated oxygen solubilities in different liquids as a function of temperature	33
3.1	Example of an adaptive PIV measurement in a vertical plane in a stirred tank, showing the radial jet flow coming from a Rushton impeller. And close-up of the boxed area in the top figure	38
3.2	Computed Bubble Shapes For Different Bubbles of Different Shapes and Sizes	41
3.3	Close-up of a PIV recording of the gas liquid flow in a bubble column, showing 16 interrogation areas of $64 \times 64 \text{ px}^2$	43
4.1	Schematic of Experimental Setup	47
4.2	A Sample Image of the Bubbles After Changing the Contrast and Brightness	49
4.3	Figure 4.3 Histogram of the Sample Image of Figure 4.2	49
4.4	An Inverted Image of a Single Bubble	50
4.5	The Process of Extracting a Single-Bubble Image from the Original Image	51
4.6	Images of Bubbles for Gas Inlet of Diameter 0.15cm	53
4.7	The Result of Running the First Program	54
4.8	The Result of Running the Second Program on a Sample Bubble Taken From the 0.15cm Gas Inlet Diameter Images	56
4.9	Specific Area Change with Gas Hold-up Change for the Three Gas Inlet Diameters	58
4.10	A Single Bubble Produced by the 0.15cm Gas Inlet	58
4.11	A Single Bubble Produced by the 0.1cm Gas Inlet	59
4.12	A Single Bubble Produced by the 0.08cm Gas Inlet	59

<b>Figure No.</b>	<b>Figure Title</b>	<b>Page</b>
4.13	Relation of $k_L$ and Gas Hold-up for the Three Gas Inlet Diameters	61
4.14	Relation of $k_L a$ and Gas Hold-up for the Three Gas Inlet Diameters	63
4.15	Experimental and Calculated Values of $\varepsilon_G$ for Gas Inlet Diameter of 0.15cm	64
4.16	Experimental and Calculated Values of $\varepsilon_G$ for Gas Inlet Diameter of 0.10cm	64
4.17	Experimental and Calculated Values of $\varepsilon_G$ for Gas Inlet Diameter of 0.08cm	65
4.18	Comparison of $k_L a$ Obtained in Thesis and $k_L a$ from a Similar Experiment	67

## ***CHAPTER ONE***

### ***INTRODUCTION***

#### **1.1 Introduction**

Most processes in the chemical process industry involve the flow and contact of multiple phases. One can for example think of the gas-particle flow in a fluidized bed or the gas-liquid flow in a bubble column.

According to Tatterson [1], 25% of all chemical reactions occur between a gas and a liquid. A major class of gas-liquid flows is the one where the liquid phase is continuous and the gas phase is dispersed in the form of bubbles.

In classical chemical reactor engineering, the reactor capacity per unit volume is often described as a number of resistances in series. These resistances are related to the transfer of components through the gas phase to the gas-liquid interface, the transfer of components from the interface into the liquid phase and the reaction of the components.

If necessary, an additional resistance due to transport from the liquid phase to the surface of a catalyst particle may be incorporated [1].

The rate-determining resistance plays an important role in the choice of reactor type for a certain process. When the reaction is the rate determining step, bubble columns are often used, because of their large liquid bulk.

Bubble columns are also used in the process of stripping or absorption. For both processes, the rate of transfer of components from the interface into the liquid phase is important. When the transfer of the component from the gas-liquid interface to the bulk of the liquid is rate determining, the reactor capacity can be increased through the use of a stirrer. In order to obtain an in depth understanding of the performance of the reactor, detailed knowledge of the hydrodynamics is vital.

The hydrodynamics of one of the most common types of gas-liquid reactors is the subject of this thesis; the bubble column. The hydrodynamics of these reactor types are studied through experiments and numerical simulations.

## **1.2 The Usage of Computers in Experiments**

Computers became a vital part of our everyday life. Chemical engineering is no different. Computers have become an important instrument in the acquisition, evaluation and analyzing of chemical engineering data.

Computational fluid dynamics (CFD) is a tool that is increasingly used in the design, scale-up, and optimization and trouble-shooting of chemical reactors. In this thesis, several aspects of CFD for gas-liquid flows in chemical reactors were studied.

Figure 1.1 shows an example of the usage of computers in obtaining and analyzing the data from a bubble column.

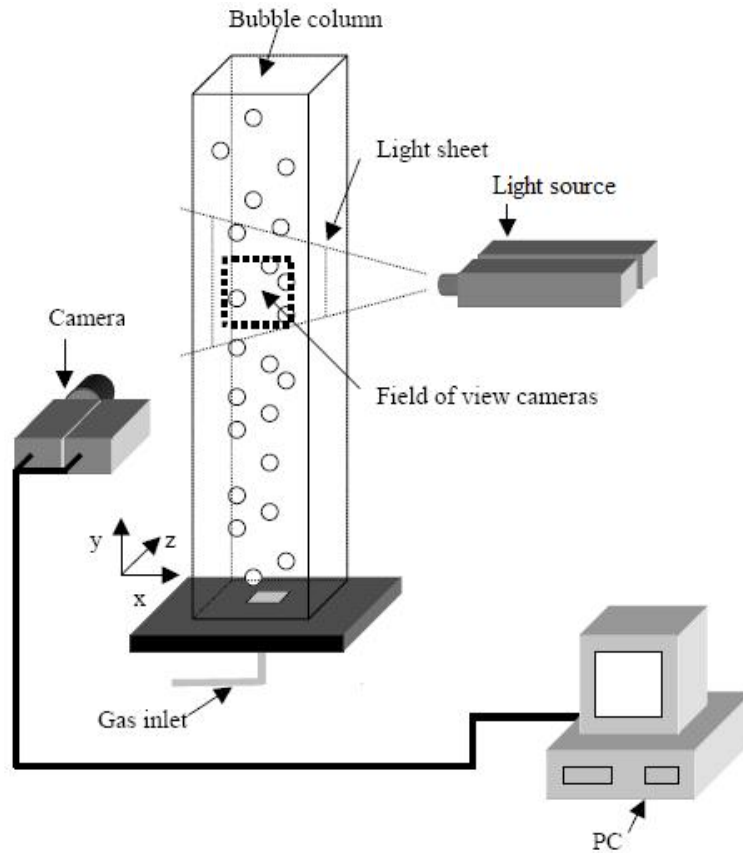


**Figure 1.1 Using Computers in Obtaining Data from Bubble Column**

[2]

The information is obtained from a chemical reactor system into a computer can be used in many types of calculations and analyses for better understanding and using a chemical reactor system.

### **1.3 Literature Survey**

In 1974, Akita and Yoshida introduced one of the earliest detailed studies of the bubble column hydrodynamics Akita, K., Yoshida, F., [2]. Their study concentrated on classical ways to study three parameters only; bubble size, interfacial area, and liquid phase mass transfer coefficient.

Fukuma, Muroyama, and Yasunishi introduced, in 1987, another detailed study that concentrated on gas-liquid interfacial area and liquid-phase mass transfer coefficient Fukuma M., Muroyama K., Yasunishi A., [3].

As the years passed, the computers started to get into this field of study in a very advantageous way. Calculations started to get easier and the images processed by the computer were more accurate and more powerful calculations were available. Adrian, R. J., [4], in 1991, introduced a study that was one of the building blocks for particle-imaging techniques for experimental fluid mechanics. His study paved the way for other studies to make great use of these techniques in studying the gas-liquid hydrodynamics and introducing better imaging techniques.

Becker, Sokolichin, and Eigenberger [5] introduced a detailed comparison and flow simulations of different experimental techniques of studying gas-liquid flow in bubble columns and loop reactors in 1994. This experimental

comparison provided researcher a good background of each technique strengths and weaknesses.

In 10th International Symposium on Applications of Laser Techniques to Fluid Mechanics in Lisbon, Portugal, 2000, two major contributions were introduced. Broder and Sommerfeld [6] introduced the use of a laser based technique called Particle Image Velocimetry (PIV) for analyzing bubbly flows. Also, Deen, Hjertager, and Solberg [7] introduced a detailed comparison of the most well-known two laser-based techniques; PIV, and Laser Doppler Anemometry (LDA). The later paper was focused on the gas-liquid flow in a bubble column. And it was the base for the PhD thesis of Niels Deen [8] in 2001. Deen provided a thorough experimental study of Fluid Dynamics in Gas-Liquid Chemical Reactors. Reference Deen, N. G., [8] became a milestone for most of the studies performed thereafter.

Also in 2001, Lain, Broder, and Sommerfeld [9] introduced numerical simulations of the hydrodynamics in a bubble column. Their study provided quantitative comparisons with experiments.

Grau and Heiskanen in 2002 [10] introduced a study that concentrated visual techniques for measuring bubble size in flotation machines.

All of the studies mentioned above and other research papers and theses have built an excellent background for researchers approaching the study of

the hydrodynamics of gas-liquid mass transfer in bubble columns and reactors.

#### **1.4 Project Aim and Contributions**

This thesis aimed to provide a simplified method to study the hydrodynamics of gas-liquid bubble column. This is done through taking photos of the gas-liquid interaction and processing these photos to extract gas hold-up and interfacial surface area of the bubble.

This information is then used to calculate other gas-liquid hydrodynamics such as the specific-area and mass-transfer coefficient, in order to provide a better understanding of the bubble column gas-liquid interaction.

This aim is achieved using simple, in-expensive, yet accurate experimental instruments.

#### **1.5 Thesis Layout**

The first chapter of this thesis provides a simple introduction to the subject of the thesis along with a focused literature survey.

Chapter two gives a brief introduction about gas-liquid mass transfer in its hydrodynamics.

The most modern techniques to analyze gas-liquid interaction in bubble columns used in the world are described in chapter three.

Implementation environment and techniques are explained in detail along with the implementation results and their discussions are introduced in chapter four.

Chapter five finalizes the work of this thesis with conclusions and suggestions for future work.

**CHAPTER TWO**  
**GAS-LIQUID MASS TRANSFER**

**2.1 Introduction to Gas-Liquid Mass Transfer**

Mass transfer between gas and liquid is a basic fundamental phenomenon in process engineering. Chemical engineering operations can be divided into three different transfer phenomena: momentum, heat and mass transfer, which are presented with the same basic relation between driving force and resistance:

$$Flux = \frac{Driving\ Force}{Resistance} \quad (2.1)$$

The basic equation to present mass transfer between gas and liquid can be written as:

$$\frac{\partial C}{\partial t} + v_L \nabla C = D \nabla^2 C + R \quad (2.2)$$

where  $C$  is the concentration of absorbed gas  $A$ ,  $t$  time,  $v_L$  liquid velocity,  $D$  ( $m^2/s$ ) diffusion coefficient of gas  $A$  and  $R$  the consumption of gas  $A$  in reaction when present Merchuk J.C., [11]. Since Equation 2.2 cannot generally be solved analytically and the boundary values are undefined, several models for mass transfer at the gas-liquid interface have been proposed. These models simplify the microscopic phenomena at the

interface. The assumptions of the models include values known as the parameters (in this case, for example, time and distance).

The well-known Fick's Law for molecular diffusion  $J_A$  (mol/m<sup>2</sup>s) can be written as follows:

$$J = -D\left(\frac{dC}{dx}\right) \cong \frac{D}{\delta}(C_G - C_L) \quad (2.3)$$

The driving force of the molecular diffusion is the concentration difference between gas  $C_G$  and liquid  $C_L$  side of the interface over the film thickness  $dx$  or  $\delta$ (m) of the layer. The mass transfer coefficient  $K$  (m/s) is defined by dividing the diffusion coefficient  $D$  by the thickness of the film  $\delta$  as follows:

$$K = \frac{D}{\delta} \quad (2.4)$$

The mass transfer coefficient  $K$  can be expressed into gas  $k_G$  and liquid  $k_L$  side mass transfer coefficients (Equations 2.5 and 2.6):

$$k_G = \frac{D_G}{\delta_G} \quad (2.5)$$

$$k_L = \frac{D_L}{\delta_L} \quad (2.6)$$

Combining Equations 2.3 and 2.4 gives the rewritten mass transfer flux of gas  $A$  through interface:

$$J_A = K(\Delta C) \quad (2.7)$$

where the mass transfer coefficient  $K$  consists of both gas and liquid side transfer coefficients as follows:

$$\frac{1}{K} = \frac{1}{Ek_G} + \frac{1}{k_L} \quad (2.8)$$

where  $E$  is the angular coefficient in the saturation curve. If  $k_G E \ll k_L$ , the gas side mass transfer controls the total transfer. It is commonly accepted Cussler, E. L., [12] that the greater resistance for mass transfer is on the liquid side and  $k_L \ll k_G E$ , Figure 2.1 shows a schematic picture of the gas-liquid interface.

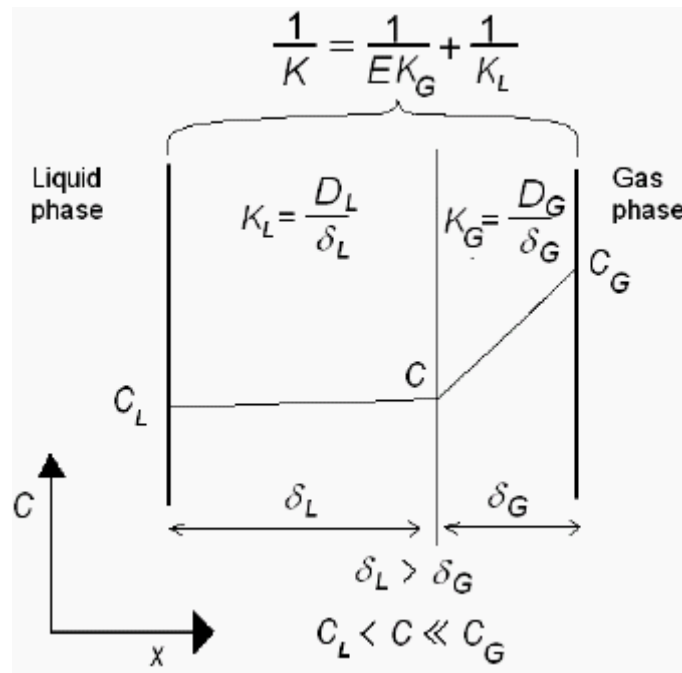


**Figure 2.1 Schematic presentation of the gas-liquid interface, concentrations and the mass transfer coefficients  $K$ ,  $k_L$  and  $k_G$  [12]**

This implies that  $K \approx k_L$  and the formula of Fick's Law (2.3) for gas and liquid mass transfer flux can be written as:

$$J \cong \frac{D_L}{\delta_L} (\Delta C) \cong k_L (C - C_L) \quad (2.9)$$

where the driving force is the concentration difference between saturated concentration of the gas in the bulk liquid  $C_L$  and concentration  $C$  in the liquid at the gas-liquid interface. If gas dissolves in the liquid without reacting, it is found experimentally that the rate of absorption of gas  $A$  is given as follows Danckwerts, P. W., [13]:

$$N_A = k_L \frac{A}{V} \Delta C = k_L a \Delta C \quad (2.10)$$

where  $N$  (mol/m<sup>3</sup>s) is the mass transfer rate and  $a$  (m<sup>2</sup>/m<sup>3</sup>) is the gas-liquid interfacial area  $A$  per unit volume of fluid  $V$ . In experimental determinations, the parameters  $k_L$  and  $a$  are often combined as the volumetric liquid mass transfer coefficient  $k_L a$ , which is usually presented as a function of process parameters.

## 2.2 Models

In this section, three types of models are introduced; film model, penetration model, and surface removal model.

### 2.2.1 Film Model

The film model, proposed by Whitman, W. G., [14], pictures a stagnant film of thickness  $\delta$  at the surface of the liquid next to the gas. While the rest of the liquid is kept uniform in composition by agitation, the concentration in the film falls from  $C_0$  at its surface to  $C_L$  at its inner edge; there is no convection in the film so dissolved gas crosses the film by molecular diffusion alone, see Figure 2.2.

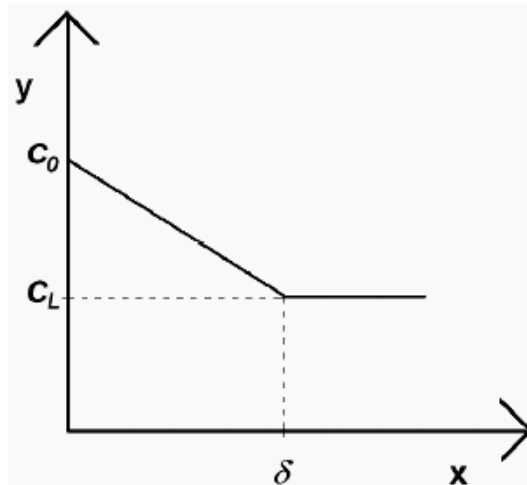


**Figure 2.2 Concentration change in film model [14]**

In the film model, the constant boundary concentrations at the boundary layer are:  $x = 0 \Rightarrow C = C_0$  and  $x = \delta \Rightarrow C = C_L$ . The concentration as a linear relation across the layer  $0 \leq x \leq \delta$  can be written as:

$$C = -(C_0 - C_L) \frac{x}{\delta} + C_0 \quad (2.11)$$

The molecular diffusion flux can be written as Equation (2.3):

$$J = -D \left( \frac{dC}{dx} \right)_{x=0} = \frac{D_L}{\delta} (C_0 - C_L)$$

while the film model leads to:

$$k_L = \frac{D_L}{\delta}$$

The assumption of a stagnant, laminar-flow film next to the boundary in which the mass transfer resistance is highest is not appropriate under many practical flow conditions, which require the application of the Fick's law for unsteady-state diffusion given below Moo-Young, M., Blanch, H. W., [15]:

$$\frac{\partial C}{\partial t} = D \frac{\partial^2 C}{\partial x^2} \quad (2.12)$$

where chemical reactions are negligible. To solve this equation, simplifying assumptions must be made, especially with regard to fluid behavior.

### **2.2.2 Penetration Model**

Higbie, R., [16] solved this problem according to the penetration model introduced, which assumes that every element of surface is exposed to the gas for the same length of time,  $\theta$ , before being replaced by liquid of the bulk composition. The model assumes that the composition of the film does not stay stagnant as in the film model Merchuk, J. C., [11]. During this short

time, the element of liquid absorbs the same amount of gas per unit area as though it were stagnant and infinitely deep. The exposure time of  $\theta$  is determined by the hydrodynamic properties of the system and is the only parameter required to account for their effect on the transfer coefficient  $k_L$ . Using appropriate boundary conditions: when  $x = 0$  then  $C = C_0$  at  $0 < t < \theta$  and when  $x > 0$  then  $C = C_L$  at  $t = 0$  and when  $0 < t < \theta$  then  $x = \infty$  and  $C = C_L$ , it was deduced that the mass transfer coefficient takes the form:

$$k_L = 2\sqrt{\frac{D}{\pi\theta}} \quad (2.13)$$

Mass transfer is dependent on the physical properties of the liquid and also the dynamics of the liquid, e.g., contact time  $\theta$ .

### 2.2.3 Surface Removal Model

Danckwerts, P. W., [13] questioned the hypothesis of a constant exposure time and postulated a random continuous renewal of surface elements at the interface according to reference's "Surface Renewal" as a more realistic situation. Introducing the statistical parameter  $s$  and found that:

$$k_L \propto \sqrt{sD} \quad (2.14)$$

The difference from the penetration model is the contact time, which is not constant but can change. Mathematically, the difference is the boundary

value of the contact time, which is not limited in the surface renewal model Merchuk, J. C., [11]. Reference Toor, H. I., Marchello, J. M., [17] proposed a film-penetration model, in which a stagnant film of definite thickness exists at the surface, but is replaced piecewise from time to time by liquid having the bulk composition. If all the parameters are kept constant, then models correlate with the equation as follows:

$$k_L = \alpha D^n \quad (2.15)$$

where the value  $n$  gets the following values:  $n = 1$  in the film model,  $n = 0.5$  represents both penetration and surface renewal model and the film-penetration model can get values  $0.5 < n < 1$ . Experimentally determined values were found as well between  $0.5 < n < 1$  [18]. See also Table 2.1 of the collected data of the models.

**Table 2.1 Collected data of the Film, Penetration and Surface removal models[18]**

Model	Film	Penetration	Surface removal
Presented	Whitman (1923)	Higbie (1935)	Danckwerts (1951)
Coefficient $k_L$	$k_L = \frac{D}{\delta}$	$k_L = \sqrt{\frac{4D}{\pi\theta}}$	$k_L = \sqrt{sD}$
Time dependence	No	Constant	Functional
Boundary conditions	$x = 0 \Rightarrow C = C_0$ $x = \delta \Rightarrow C = C_L$	When $x = 0$ and $t = 0$ then $C = C_L$ or $0 < t < \theta$ then $C = C_0$ . When $x = \infty$ and $0 < t < \theta$ then $C = C_L$	When $x = 0$ and $t = 0$ then $C = C_L$ . or $0 < t < \infty$ then $C = C_0$ . When $x = \infty$ and $0 < t < \infty$ then $C = C_L$

### 2.3 Factors Affecting Gas-Liquid Mass Transfer

The processes are usually operated according to optimum temperature, pressure, mixing, concentrations and the way of introducing the substances. To understand the hydrodynamic factors affecting the mass transfer rate, Equation (2.11) is divided into the following parts: volumetric liquid mass transfer coefficient  $k_L a$ , liquid mass transfer coefficient  $k_L$ , gas-

liquid interfacial area per liquid volume  $a$ , concentration driving force  $\Delta C$ , superficial gas and liquid velocity  $V_s$ , and gas hold-up  $\varepsilon$ , see Figure 2.3.

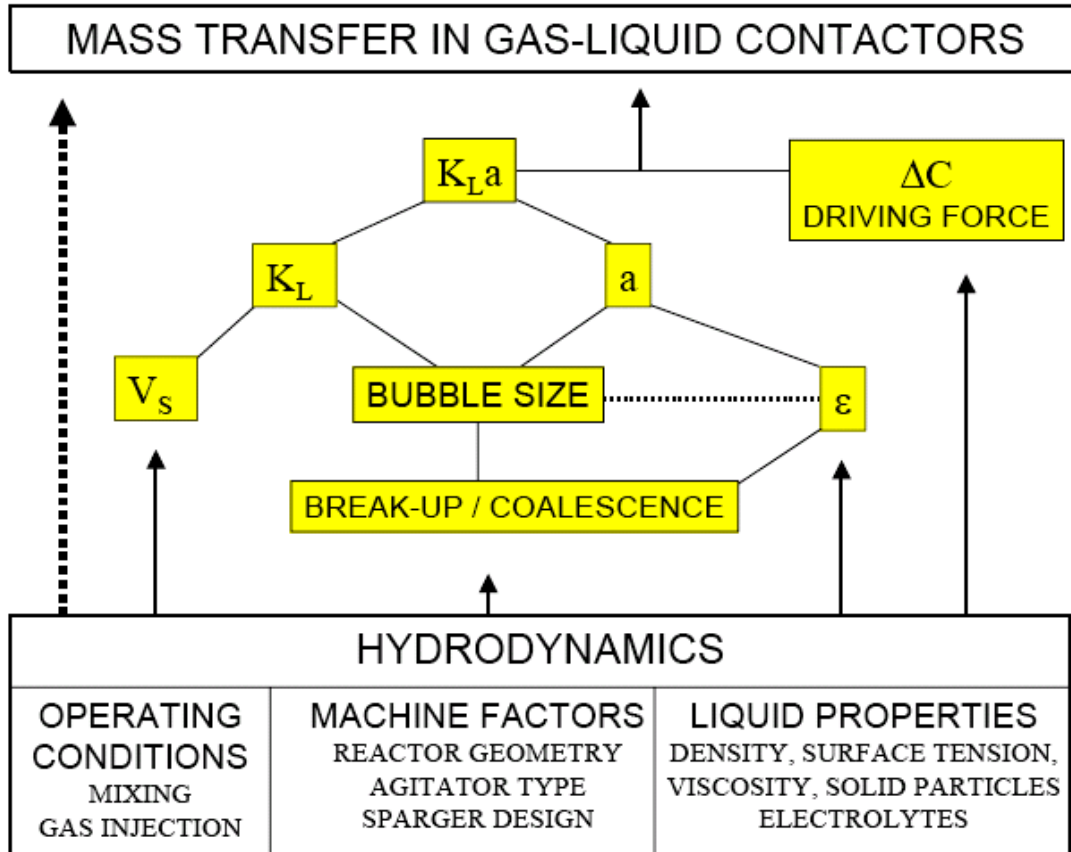


**Figure 2.3 Factors Affecting the Mass Transfer Rates in a Gas-Liquid Reactor**

The overall mass transfer rate is complex and influenced by a number of physical parameters, operating conditions and machine factors [18]. Each term has a special effect on and is therefore discussed separately.

### 2.3.1 Volumetric Liquid Mass Transfer Coefficient, $k_L a$

In experimental determinations, the parameters  $k_L$  and  $a$  are often combined as the volumetric liquid mass transfer coefficient  $k_L a$ , which is usually presented as a function of process parameters. In practice, it is usually not possible to determine  $k_L$  and  $a$  separately by measurements of physical absorption, but it is possible in the case of  $k_L a$ , where process parameters represent operating parameters such as power input  $P$ , volume  $V_L$  and gas superficial flow rate  $v_G$ . Volumetric liquid mass transfer coefficient  $k_L a$  values are often presented to within a  $\pm 30\%$  error level as follows Kaskiala, T., [18] and Van't Riet, k., [19]:

$$k_L a = \kappa \left( \frac{P}{V_L} \right)^\alpha v_G^\beta \quad (2.16)$$

where  $K$  is constant and  $\alpha$  and  $\beta$  are exponents. The values for  $\alpha$  and  $\beta$  show a great variation:  $0.4 < \alpha < 1$  and  $0 < \beta < 0.7$ . It is not unusual for the  $K$  value to remain unmentioned Van't Riet, K., [19].

The volumetric mass transfer coefficient increases significantly when ion concentration in the solution is raised. The addition of electrolyte increases the gas hold-up, due to its influence on decreasing bubble size and the non-coalescence effect at both low and high pressures Wilkinson, P. M. Haringa, H., Van Dierendonck, L. L. [20]. Once a limit for non-coalescence concentration has been reached, the increase is much smaller. The

distinction depends on  $P/V$  and  $v_G$ . It increases at higher  $P/V$  values, hence the  $k_L a$ 's for ionic solutions are more dependent on  $P/V$  than those for pure water K. Van't Riet [19]. Volumetric mass transfer correlations are also dependent on the reactor type applied. For example, Kaskiala, T. [18] proved an increase of  $k_L a$  with increasing pressure by the increase in total gas hold-up. Therefore, with high reactors, the hydrostatic pressure can be assumed to have an effect on  $k_L a$ . K. Van't Riet [19], on the subject of correlation with  $P/V$ , stated that there is no influence of stirrer geometry and the number of stirrers on mass transfer in non-viscous systems. However, Wilkinson, P. M., Haringa, H., Van Dierendonck, L. L. [20] were able to increase the mass-transfer rate 17% by changing the impeller. According to Kaskiala, T. [18], the  $k_L a$  value decreased with increasing the liquid viscosity and increased with temperature. Zhu, Y., Wu, J. [21] stated also increasing of  $k_L a$  value with increasing temperature between approximately 25-60 °C and decreasing of  $k_L a$  value with increasing temperature between approximately 60-80 °C. According to Zhu, Y., Wu, J., [21] and Yang, W. Wang, J., Jin, J. [22], solid particles can have an opposing effect on gas-liquid mass transfer,  $k_L a$ . High concentrations of fine particles increase the apparent viscosity, decreasing  $k_L$  and  $a$ .

Very small particles, which stay at the interface, can decrease interface mobility, decreasing the change of coalescence, thereby increasing  $a$ , but decreasing  $k_L$ . However, small particles could also give premature film rupture, thus enhancing coalescence and decreasing  $a$ . Larger particles could collide with bubbles and distort them until they break, thereby increasing  $k_L$  and  $a$ . Rautio, M. [23] found experimentally that increasing solid concentrations of up to 10 vol-% decreased  $k_L a$  values by 30% compared to pure water and, with 40 vol-% of solid, the decreasing was already 60% smaller. It should also be stressed that none of the overall correlations for  $k_L a$  has universal applicability Moo-Young, M., Blanch, H.W. [15]. Therefore, to explain further the gas- liquid mass transfer phenomena, it is important to study the behavior of  $k_L$  and  $a$  independently.

### **2.3.2 Liquid Side Mass Transfer Coefficient, $k_L$**

The liquid side mass transfer coefficient,  $k_L$ , measures the rate at which molecules move through an interfacial boundary layer.

- Temperature (viscosity, density, surface tension)
- Mixing conditions (stirrer and reactor)
- Size of the molecules
- Surface active substances

Increasing the mass transfer coefficient is possible by either reducing the size of the boundary layer or increasing the rate at which molecules move through the boundary layer. Increasing the turbulence decreases the boundary layer. Increasing the temperature increases the diffusivity and reduces the boundary layer Merchuk, J. C., [11] and Yang, W. Wang, J., Jin, J. [22]. An increase in temperature results in an increase in  $k_L$  Moo-Young, M., Blanch, H.W. [15]. Numerous studies on mass transfer in the bubble column have revealed that the mass-transfer coefficient  $k_L$  depends mainly on the mean bubble size, physical properties of the liquid medium, and the diffusivity of the absorbing gas component in the liquid medium.

The bubble size influences significantly the value of the mass transfer coefficient,  $k_L$ . According to Kaskiala, T. [18], it is possible to distinguish between the effect of so-called tiny bubbles,  $d_s < 0.002$  m, and of large bubbles,  $d_s > 0.002$  m. For tiny bubbles, values increase rapidly with bubble size from constant initial value  $k_L = 1 \times 10^{-4}$  m/s corresponding to  $d_s \leq 0.0008$  m to  $k_L \cong 5 \times 10^{-4}$  m/s corresponding to  $d_s \cong 0.002$  m. In the region of large bubbles, values of the mass transfer coefficient decrease slightly with increasing bubble diameter to the value of  $k_L \cong (3-4) \times 10^{-4}$  m/s. The bubble-size effect should be employed with caution, especially if bubble size is decreased with the use of a surface active agent (e.g., electrolytes, polymers,

antifoams, oils, alcohol and small particles) when the  $k_L$  is influenced strongly by interfacial phenomena as well. Since the addition of surface active substances reduces the rate of renewal of the surface elements at the interface, it negatively affects the mass transfer from the bubbles. In general though, surface active agents increase  $a$  by increasing  $\varepsilon_G$  and decreasing  $d_b$ , by an even larger factor, so that  $k_L a$  usually increases, though occasionally it has been found to decrease Kaskiala, T. [18]. Several correlations for the mass transfer coefficient in mechanically agitated reactors exist in the literature, as in, for example:

P.W. Danckwerts, P.W. [13]:

$$k_L = 0.423 \sqrt[3]{\frac{\mu_L g}{\rho_L}} \sqrt[2]{\frac{D_L \rho_L}{\mu_L}} \quad (2.17)$$

and:

$$k_L = 0.423 \sqrt[3]{\frac{(\rho_L - \rho_G) \mu_L g}{\rho_L^2}} \sqrt[2]{\frac{D_L \rho_L}{\mu_L}} \quad d_b > 2.5 \text{mm} \quad (2.18)$$

$$k_L = 0.313 \sqrt[3]{\left(\frac{(\rho_L - \rho_G) \mu_L g}{\rho_L^2}\right)^2} \sqrt[2]{\frac{D_L \rho_L}{\mu_L}} \quad d_b < 2.5 \text{mm} \quad (2.19)$$

For bubble columns the correlation for  $k_L$  was proposed as follows by Akita, K., Yoshida, F., [2]:

$$k_L = \sqrt[2]{D_L d_b} \sqrt[8]{\left(\frac{\rho_L}{\gamma}\right)^3} \quad (2.20)$$

According to several authors,  $k_L$  values between oxygen and water at STP ranged between  $(1-6)\times 10^{-4}$  m/s. Moo-Young, M., Blanch, H.W. [15] reported, for example, the exact value of  $1.35\times 10^{-4}$  (m/s).

### 2.3.3 Specific Gas-Liquid Interface Area, $a$

The value of  $a$  can be evaluated from the mean gas hold-up,  $\varepsilon_G$ , and the volume surface mean bubble diameter,  $d_b$ , as follows [15]:

$$a = \frac{6\varepsilon_G}{d_b} \quad (2.21)$$

The total gas-liquid interfacial area in liquid volume  $a$  is determined by the size, shape and number of the bubbles. Factors affecting the size of the bubbles include:

- Stirring speed and type of the impeller
- Reactor design
- The way the substances are introduced
- Medium composition (e.g., the presence of surface active agents)

The interfacial area can be increased by creating smaller bubbles or increasing the number of bubbles. For a given volume of gas, a greater interfacial area,  $a$ , is provided if the gas is dispersed into many small bubbles rather than a few large ones. The stirrer and the mixing intensity play a

major role in breaking up the bubbles. Reactor design effects the gas dispersion, hold-up and residence time of the bubbles. Baffles are used to create turbulence and shear, which break up the bubbles.

The properties of the medium also affect significantly the bubble sizes and coalescence and therefore the interfacial area. When the solution contains electrolytes, it was found that electrolytes decrease the dissolved gas concentration, which in turn decreases the strength of the attraction between bubbles mediated by micro bubbles; this inhibits coalescence. Sada, E. Kumazawa, H. Lee, L.H. Iguchi, T. [24] showed that, with particles finer than  $10\mu\text{m}$ , the bubble coalescence was hindered and the bubble interfacial area and hold-up was increased; with particles larger than  $50\mu\text{m}$ , the effects were the opposite. O'Conner, C.T. Randall, E.W. Goodall, C.M. [25] reported bubble size increased with the particle size of the ore, pulp density and air flow rate. An increase in temperature reduced bubble size, as did reduced viscosity.

In the literature, there are several correlations for bubble sizes, which can be divided into categories of bubbles generated at an orifice and bubbles far from the orifice. Previous studies by Kaskiala, T. [18] on the mechanism of bubble formation show that, depending on the controlling mechanisms, one can distinguish between:

- Surface tension controlled by bubble detachment diameter.
- Viscous drag controlled by bubble detachment diameter.
- Liquid inertia controlled by bubble diameter.

The surface tension and viscous forces are two major contributing forces influencing the bubble diameter during its formation. It was observed that the surface tension is one of the major parameters contributing to the bubble volume, and that it should be taken into consideration even at high gas flow rates. On the other hand, the viscous force is only important at high gas flow rates and can be ignored at low flow rates. The orifice diameter  $d_0$  influences the bubble size strongly only at very low gas-flow rates, where the bubble size is found by equating surface tension and buoyancy forces Moo-Young, M., Blanch, H.W. [15]:

$$d_b = \sqrt[3]{\frac{6\sigma d_0}{g(\rho_L - \rho_G)}} \quad (2.22)$$

The gas rates for which this equation is valid are too small to be of practical interest. At high gas-flow rate, in the case of liquids with low viscosity, the effect of surface tension is generally considered negligible. In the region of the tank away from the orifice, the bubble size may vary, depending on the liquid properties and the liquid motions generated by the rising gas stream. If the power input from the gas phase is insufficient to generate turbulence in

the liquid phase, the bubble size in the tank will be that of bubbles formed at the orifice, and may increase with liquid height in the tank due to bubble coalescence. Once the liquid is in turbulent motion, however, bubble break-up will also occur, and equilibrium between coalescence and break-up will determine the mean bubble size.

In the case of preheated gas injection, Kaskiala, T. [18] found a decrease in the bubble diameter which was associated with increasing temperature.

A correlation between the oxygen solubility and transition concentration suggested that dissolved gas concentration has an important influence on the interaction between two bubbles, but a contribution due to the Gibbs-Marangoni effect and surface elasticity cannot be ruled out. Reference Kaskiala, T. [18] stated that increasing pressure decreases bubble size and hold-up. For fixed pressure and gas velocity the temperature effect on gas hold-up is complex, but an increase in temperature generally increases the gas hold-up. This general trend is due to the dominant role of the associated reduction in liquid viscosity and surface tension, which leads to smaller bubble size. The associated gas density often plays a secondary role. Reference Zhu, Y. Wu, J. [21] stated that the hold-up of the air water systems increases slowly at temperature  $T < 75^\circ \text{C}$  and remarkably at  $T > 75^\circ \text{C}$  and is related to the vapor pressure of the gas.

### **2.3.4 The Diffusional Driving Force, $\Delta C$**

The driving force is the gradient between the concentration of the substance at the boundary layer and in the bulk liquid (average concentration). Factors affecting this gradient include:

- The solubility of the gas
- Metabolic activity

Higher solubilities can be achieved by increasing the partial pressure of the gas. The presence of one solute may affect the solubility of another. The salting-out effect is the reduction of the solubility of a gas in water when such a salt is added. Solubility has a minimum point as a function of temperature. In case of water, the minimum is close to the boiling point of water. Solubility is dependent on, for example, temperature, pressure, salts present and chemical reactions. Metabolic activity, on the other hand, uses the substrate and therefore decreases the concentration in the bulk liquid ( $C$ ), again increasing the driving force across the boundary layer.

When it comes to determining the rate-limiting step for bubble dissolution, there are different opinions. Adrian, R. J., [4] showed by means of three-

component gas bubble tests that solubility is the major effect that causes bubble dissolution in the early time of the dissolution process. For intermediate and longer times, the rate of diffusion interacts with the solubility to control the rate of bubble shrinkage. On the other hand, Moo-Young, M., Blanch, H.W. [15] assumed that the rate-limiting step for bubble dissolution is diffusion of gas in the fluid rather than interfacial mass transport.

## **2.4 Solubility of Gases in Liquids**

The solubility of a particular solute in a solvent is the maximum amount of solute that will dissolve in a specified amount of solution or solvent. It represents the saturated level of the solution where no more solute will dissolve within the solution. This saturated condition is a physical equilibrium between the solute and solvent and the solution. Unsaturated solutions are those that are below the solubility limits of the solute in that solvent, while supersaturated solutions are above the solubility limits. Supersaturated solutions are nonstable. Such solutions will have the excess solute crystallize out with any disturbance of the supersaturated solution establishing a saturated solution. Measurements or investigations of oxygen solubility in water and aqueous solutions have been done for many decades

Kaskiala, T. [18] and the factors affecting the solubility are well known. Models and theories based on different assumptions for estimating the activities in solutions have been created. Theories for aqueous solutions with strong electrolytes have been presented by, for example, Danckwerts, P.W. [13] Merchuk J.C., [11] and Fukuma M., Muroyama K., Yasunishi A., [3]. Modeling of oxygen solubility in aqueous solutions can be found Kaskiala, T. [18].

#### 2.4.1 Thermochemical Calculations

The equilibrium between molecular oxygen in the gas phase  $O_2(g)$  and oxygen dissolved in water  $O_2(aq)$  is given by the following equation [18]:

$$k = \frac{\gamma c_{aq}}{\phi P_{O_2}} = \frac{[O_2]_{aq}}{[O_2]_g} \quad (2.23)$$

where  $k$  is the equilibrium constant and  $[O_2]_{aq}$  and  $[O_2]_g$  represent the activity of  $(O_2)_{aq}$  and fugacity of  $(O_2)_g$ , respectively. When  $c_{aq}$  is proportional to  $P_{O_2}$ , the solute exhibits a Henry-type behavior with a proportional Henry's law constant  $H$  equilibrium; the constant may be rewritten as:

$$k = \frac{1}{H} \left( \frac{\gamma}{\phi} \right) = \frac{[O_2]_{aq}}{[O_2]_g} \quad (2.24)$$

when  $\gamma$  and  $\phi$  are close to unity such that  $\gamma/\phi=1$ , then  $k=I/H$ . This situation is expected to prevail at low-solute concentrations and moderate partial pressures of oxygen. At any temperature  $T$ ,  $k$  is related to the standard molar chemical potentials  $\mu_{aq}^o$  and  $\mu_g^o$  of the aqueous and gaseous oxygen species, respectively, at temperature  $T$  and to the overall change in standard chemical free energy of the reaction ( $\Delta G^o$ ) via Equation (2.25) leading to Equation (2.26).

$$\Delta G^o = \mu_{aq}^o - \mu_g^o = -RT \ln k \quad (2.25)$$

$$k = \exp\left\{\frac{\mu_g^o - \mu_{aq}^o}{RT}\right\} = \exp\left\{\frac{-\Delta G^o}{RT}\right\} \quad (2.26)$$

Through thermodynamic calculations, it is possible to calculate the equilibrium constants for gases and electrolytes in liquids Van't Riet, K. [19]. The computer aided multi-component calculation methods for multiphase systems, including gas solubility, have been developed in recent years.

#### **2.4.2 Gas Solubility at Elevated Temperatures**

The gas-liquid equilibrium of oxygen is described by Henry's law, the linear relationship of which is valid for dilute solutions of non-reacting systems and for gases that are weakly soluble in liquid. The temperature dependence

of Henry's constant for oxygen in water given by Fogg, P.G.T. Gerard, W. [26] is as follows:

$$\ln\left(\frac{P}{H_0}\right) = A + \frac{B}{T} + C \ln T \quad (2.27)$$

where  $H_0$  denotes the dimensionless representation of Henry's law constant in partial oxygen pressure  $P$  at 1 atm. The coefficients  $A$ ,  $B$  and  $C$  are listed in Table 2.2.

**Table 2.2 Coefficients A, B and C used for calculating Henry's constant [26]**

A	B	C	Temperature Range
-171.2542	8391.24	23.24323	273-333 K
-139.485	6889.6	18.554	273-617 K

### 2.4.3 Empirical Modeling of Gas Solubility in Electrolytic Solutions

The addition of salt to water changes its solvent properties. It can reduce or increase the solubility of gas. This phenomenon is commonly called the salting in and out effect and it is a result of molecular interactions between charged and neutral particles in a liquid solution. Increasing salt concentration, the gas solubility is nearly always found to decrease due to the salting-out effect of the ions. This effect, as derived from Henry's law

constant, can be related in Setschenow linear salting out function Kaskiala, T. [18]. At moderate high-salt concentrations, the effect of salt concentration,  $C_s$ , on the solubility,  $C_G$ , of a sparingly soluble gas as compared to that in pure water,  $C_{G,0}$  was described by Setschenov in 1889 Kaskiala, T. [18] in the following form:

$$\log\left(\frac{C_{G,0}}{C_G}\right) = KC_s \quad (2.28)$$

Parameter  $K$  (Setschenov's constant) is specific to the gas as well as to the salt and shows a moderate temperature dependency Grau, R. A. and Heiskanen, K. [10]. The relation usually holds well up to salt concentration of about 2 kmol/m<sup>3</sup> and sometimes more than 5 kmol/m<sup>3</sup>. At higher salt concentrations, the gas solubility tends to be underestimated Grau, R. A. and Heiskanen, K. [10]. The equation can also be applied for mixed electrolyte solutions as follows:

$$\log\left(\frac{C_{G,0}}{C_G}\right) = \log\left(\frac{H}{H_0}\right) = \sum_i (h_i + h_G)C_i \quad (2.29)$$

where  $C_i$  denotes the concentration of ion  $i$  in the solution and  $h_i$  is a ion-specific parameter. Grau, R. A. and Heiskanen, K. [10] extended the model of Schumpe to the temperature range 273-363 K by assuming  $h_G$ , (the gas-specific constant) as a linear function of the temperature:

$$h_G = h_{G,0} + h_T(T - 298.15) \quad (2.30)$$

where  $h_{G,0} = 0[\text{m}^3/\text{kmol}]$ ,  $h_T = -0.334 \times 10^{-3}[\text{m}^3/\text{kmol} \cdot \text{K}]$ .

Only few publications concerning measurements of the solubility of oxygen in aqueous sulphuric acid were found. With respect to the direct leaching of zinc sulphide conditions, experimental values for the oxygen solubility cannot be found. However, based on information found, good approximations are available. In this work, the gas solubility values determined by the model of Grau, R. A. and Heiskanen, K. [10] were chosen as the most suitable. Examples of the calculated oxygen solubility values can be seen in Figure 2.4.

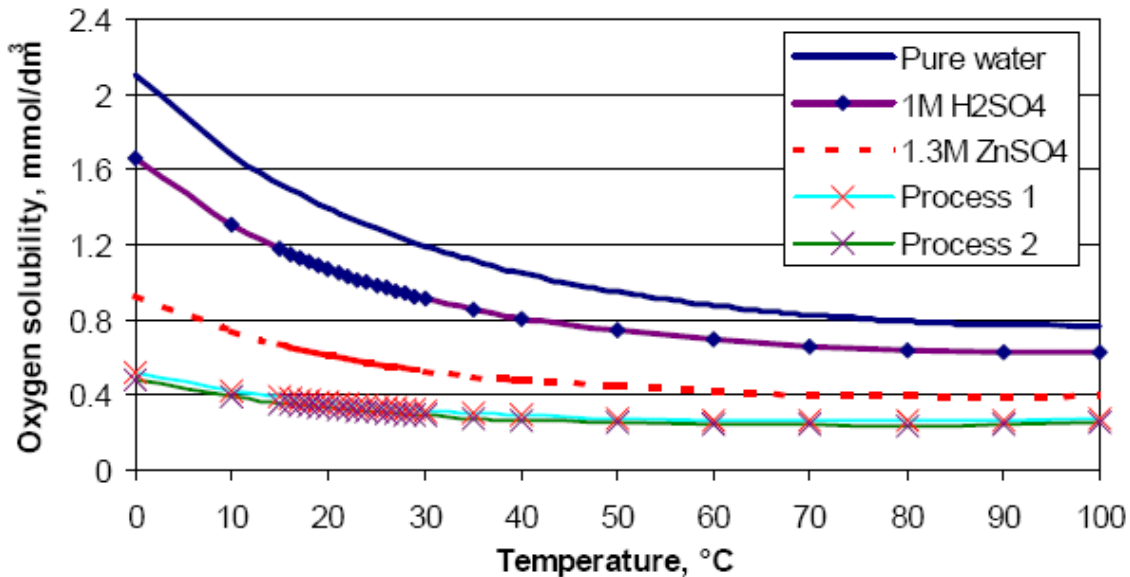


**Figure 2.4** Calculated oxygen solubilities in different liquids as a function of temperature [10]

The solubility of oxygen was calculated in water and in salt solutions containing 1 M  $\text{H}_2\text{SO}_4$  , 1.3 M  $\text{ZnSO}_4$  and two complex process solutions containing different amounts of  $\text{H}_2\text{SO}_4$ ,  $\text{ZnSO}_4$  and  $\text{Fe}_2(\text{SO}_4)_3$  . Process solution 1 contained together 3 M sulphates and solution 2 contained 2.7 M sulphates. The solubilities were calculated with the model presented. The solubility of oxygen in process solutions is significantly less than in pure water. However, the solubility of oxygen in process solution 1 and 2 were nearly the same. Increasing temperature (at a constant partial pressure) under 100°C decreases the solubility. At higher temperatures, the solubility may pass through a minimum. At a partial pressure of 1.013 bar, the solubility of oxygen in pure water passes through a minimum at about 95°C Rautio, M. [23].

**CHAPTER THREE**  
**METHODS FOR MEASURING GAS HOLD-UP**

**3.1 Introduction**

This chapter discusses experimental techniques used to acquire and process information from gas-liquid mass transfer systems using computers. In order to validate the results of computational fluid dynamics simulations, quantitative measurement data is crucial. Many different measurement techniques are available for this purpose. The most frequently used methods are laser-based. That is, particle image velocimetry and laser doppler anemometry. The advantages of these techniques are their non-intrusive character and high resolution Deen, N. G., Hjertager, B. H. & Solberg, T., [7].

**3.2 Laser Doppler Anemometry (LDA)**

LDA is one of the oldest laser-based measurement techniques in fluid dynamics. This technique is based on the interference pattern in the crossover region of two crossing laser beams. This interference pattern, also known as fringe pattern, becomes visible when particles pass the crossover region and scatter light into the direction of a receiving probe. Since the

distance between the fringes is known, the velocity can be deduced by multiplying the fringe spacing,  $\Delta x$  by the measured frequency of the fringe pattern,  $f_p$  Deen, N. G., Hjertager, B. H. & Solberg, T., [7]

$$u = \Delta x f_p \quad (3.1)$$

Although the amount of light that is scattered backward of the particles is only small, this mode of operation is often used. The reason for this is obvious: the sending and receiving probes can be combined into a single device. In the simplest mode of operation LDA is able to measure the magnitude of the velocity, but not the direction of the flow. This can be a problem for example in circulating flows where the direction of the flow is not known a priori. In order to solve this ambiguity in the velocity, Bragg cells are often used to superimpose a constant movement of the fringe pattern,  $f_f$ . The velocity can then be calculated as follows Deen, N. G., Hjertager, B. H. & Solberg, T., [7]:

$$u = \Delta x (f_p - f_f) \quad (3.2)$$

By combining up to six laser beams, the second and third velocity components can also be measured.

In a LDA measurement, data can be acquired at a very high rate. The advantage of this is that time dependent behavior can be measured very

accurately. Furthermore (turbulent) statistics of the flow can be calculated in a fast way. A disadvantage of the technique is that it is limited to a measurement at a single point. Whole field characteristics can only be measured in stationary flows. To accomplish this, expensive positioning and traversing apparatus are often necessary.

### **3.3 Particle Image Velocimetry (PIV)**

In contrary to LDA, PIV is a whole field measurement technique. To visualize the movement of the fluid, it is seeded with small tracer particles. A cross section of the flow is illuminated by a laser sheet. Next, two subsequent images of the cross section of the flow are recorded, with an exposure time delay of  $\Delta t$ . The images are then divided into small interrogation areas with approximately constant velocity. The displacement of the particles,  $\Delta x$  between two images can be determined by using correlation techniques. Finally, the velocity is calculated as follows [6]:

$$v = \frac{\Delta x}{M\Delta t} \quad (3.3)$$

where  $M$  is the magnification of the camera. When this is done for all interrogation areas of the image, it results in an instantaneous velocity field for the entire cross section of the flow.

The main difference between LDA and PIV is that the LDA is a single point measurement technique with a high temporal resolution, whereas PIV is a whole plane measurement technique, with a high spatial resolution. Keeping this in mind, the combination of the results from both techniques forms a valuable source of information to gain a thorough insight in the physical flow phenomena. Figure 3.1 shows an example of an adaptive PIV measurement in a vertical plane in a stirred tank [7].

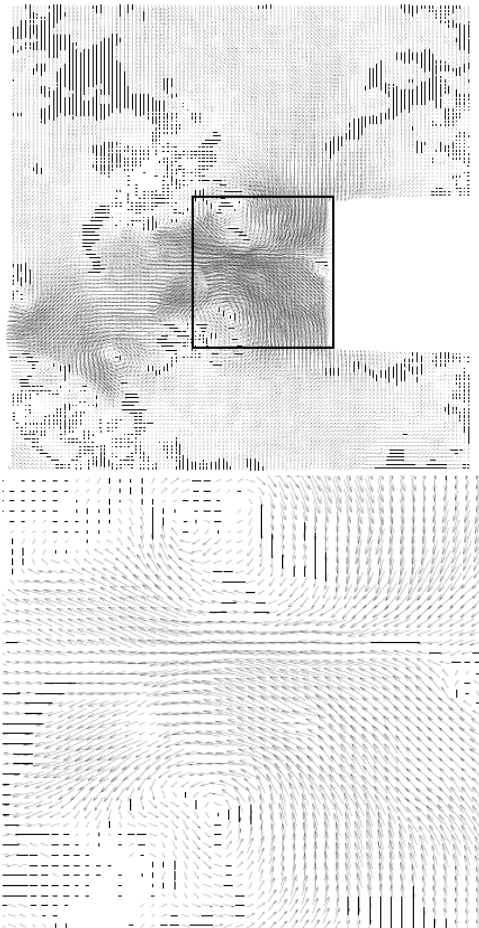


**Figure 3.1 Top: example of an adaptive PIV measurement in a vertical plane in a stirred tank, showing the radial jet flow coming from a Rushton impeller. Bottom: close-up of the boxed area in the top figure.**

### 3.4 3D Modeling of Mass Transfer

This technique van Sint Annaland, M., Dijkhuizen, W., Deen, N. G., and Kuipers, J. A. M. [27] Dadan Darmana, Niels G. Deen, J. A. M. Kuipers, [28] of studying the gas-liquid mass transfer and bubbles' behavior depends totally on computers.

In this technique a three-dimensional (3-D) front-tracking (FT) model is presented featuring a new method to evaluate the surface force model that circumvents the explicit computation of the interface curvature. This method is based on a direct calculation of the net tensile forces acting on a differential element of the interface. This model can handle a large density and viscosity ratio and a large value of the surface tension coefficient characteristic for gas-liquid systems. First, the results of a number of test cases were presented in van Sint Annaland, M., Dijkhuizen, W., Deen, N. G., and Kuipers, J. A. M. [ [27] to assess the correctness of the implementation of the interface advection and remeshing algorithms and the surface tension model. Subsequently, the computed terminal Reynolds numbers and shapes of isolated gas bubbles rising in quiescent liquids are compared with data taken from the bubble diagram of Grace. In addition drag coefficients for rising air bubbles in water were successfully computed, a system that has proven difficult to simulate by other methods, and showed

good agreement with existing correlations. A number of sample calculations involving multiple bubbles were reported in Dadan Darmana, Niels G. Deen, J. A. M. Kuipers, [28] to demonstrate the capabilities of the three-dimensional FT model. Figure 3.2 shows an example of calculated bubbles of different shapes and sizes.

### **3.5 Choosing the Experimental Technique**

Other than the ones mentioned here in this chapter, many techniques to gather information exist to study bubble column reactors as well as stirred tank ones. Choosing the technique is controlled by your needs. The type of hydrodynamics you need to study imposes the type of technique you can use.

Most of the time, you will need more than one technique to gather the data that you need about the mass transfer. This is due to the fact that each technique provides different type of information or approaches the system in a different way that gives more accurate information in one way or another.

PIV and LDA are two of the most widely used laser-based techniques. Each of these two techniques studies the particles motion, i.e. the bubbles behavior and motion. If you do not need this type of information and you need simpler information, you will need to seek a simpler technique.

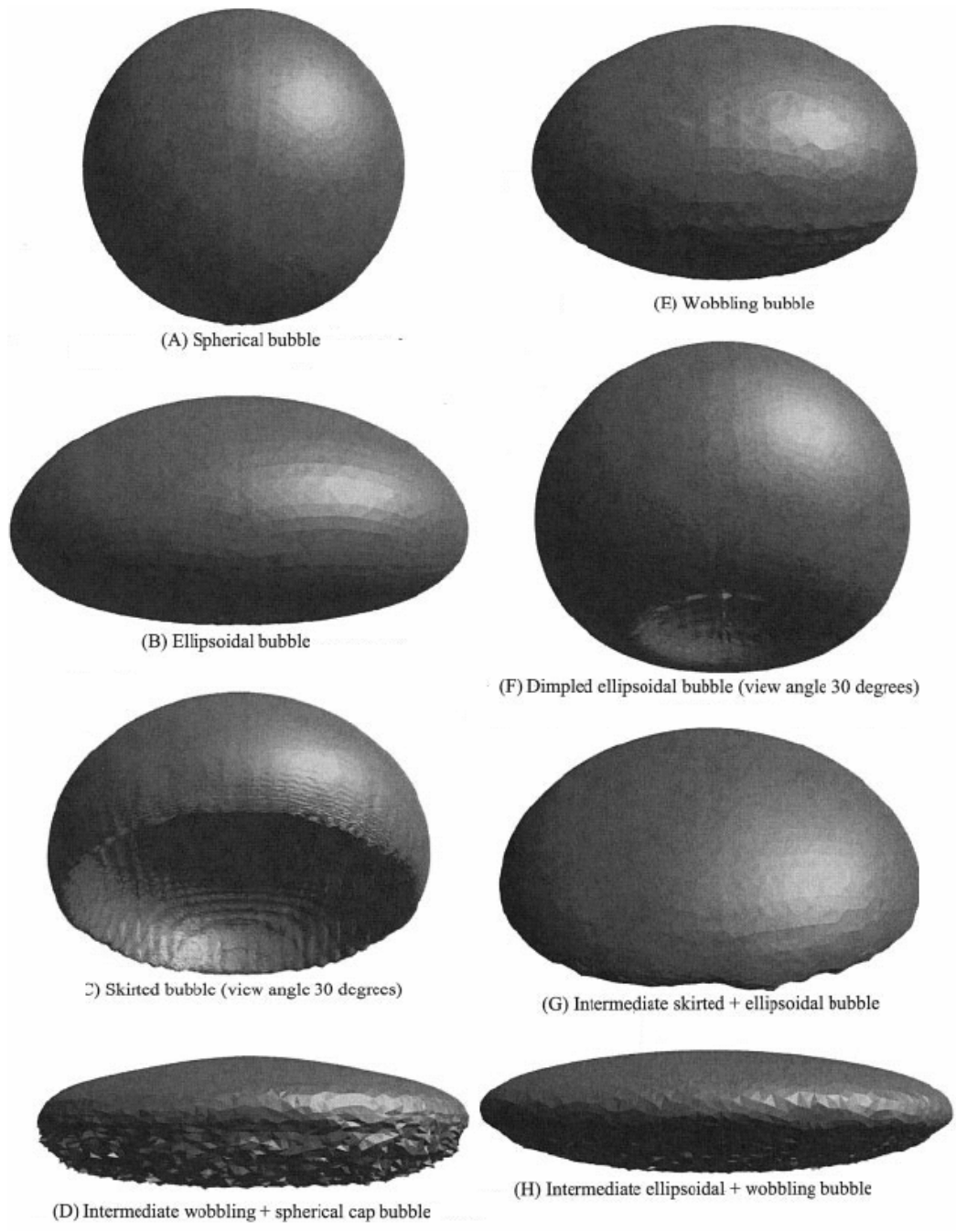


**Figure 3.2 Computed Bubble Shapes For Different Bubbles of Different Shapes and Sizes [28]**

The advantages of PIV are that velocities of two different phases can be determined simultaneously in a whole plane in the flow, without disturbing the flow. One of the major disadvantages of these techniques is the rather low temporal resolution (typically 15 Hz for digital PIV). Laser Doppler Velocimetry (LDA) on the contrary has a very high temporal resolution (typically in the order of 1 kHz). Since LDA is a single point measurement technique, one can only measure the velocity of one particle at a time. Therefore it is not possible to measure the velocities of different phases simultaneously.

Another technique is Particle Tracking Velocimetry (PTV). This technique is similar to PIV with slight differences.

First of all one should decide whether one should use PTV or PIV for each of the phases. To make this decision, one can use the following explanation Deen, N. G., Hjertager, B. H. & Solberg, T., [7]. In PTV, the average distance between the particles is much larger than the mean displacement. That means that the displacement of particles can easily be determined, without confusing them with neighboring particles. Meanwhile the number of particles per interrogation area (i.e. a small area, in which the velocity is to be determined) is too small to apply PIV. At least four to five particles per interrogation area are needed to determine the velocity with PIV. So,

depending on the flow system under consideration one should decide to process the images with PTV or PIV algorithms. In some cases this choice is not obvious, because there can be a wide range of particle concentrations, differing from one interrogation area to another. This is illustrated in Figure 3.3. In this figure a close-up of a PIV recording of the gas-liquid flow in a bubble column is shown. It can be seen that in interrogation area D3 there are only tracer particles present, while the entire interrogation area C1 is filled with bubbles. In each area only the velocity of one phase can be determined.

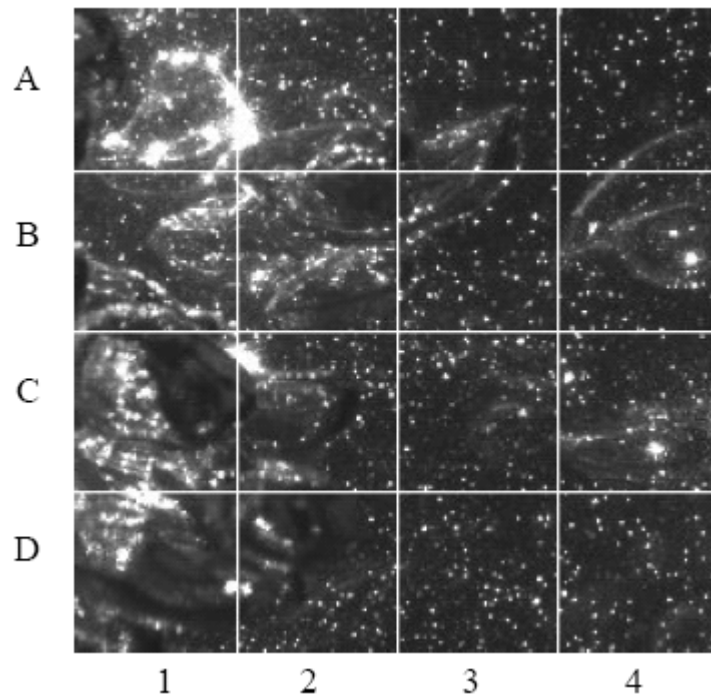


**Figure 3.3 Close-up of a PIV recording of the gas liquid flow in a bubble column, showing 16 interrogation areas of  $64 \times 64 \text{ px}^2$  [7]**

Many experiments used PTV for both the dispersed and the continuous phase. An important aspect in the processing of the images is the identification of the dispersed phase. Some experiment performed measurements of both the gas and the liquid phase in a system of single bubbles rising in a heavy mineral oil. In order to be able to detect the particle images, the bubbles needed to be overexposed. The bubble images consisted of overexposed round spots. A threshold function was used to determine the position of the edges of the bubble. Then both the tracer particles and the bubbles were tracked. In order to obtain a velocity field on a regular grid, the PTV data was interpolated. Since the seeding density in PTV is much lower than in PIV, a much lower spatial resolution can be obtained.

## ***CHAPTER FOUR***

### ***IMPLEMENTATION AND RESULTS***

#### **4.1 Introduction**

This chapter presents the technique that was used to gain and process information from a bubble column. The two parameters investigated in this thesis do not require the complex operations mentioned in chapter three. These parameters are the gas hold-up and the interfacial area of one bubble. To obtain these two parameters, an experiment was done using simple inexpensive apparatus with easily obtainable software to process the acquired data and process the images. The following sections will describe this experiment in detail.

#### **4.2 Apparatus Used**

The following apparatus was used to perform the experiments:

1. Bubble Column:

A transparent glass duct was used as the bubble column. Its dimensions were 10x10x50cm. Its base was a steel square with a small hole in the middle acting as the gas inlet. The gas inlet size was changed for three

different readings. The diameter of the gas inlet used was 0.15, 0.1, and 0.08 cm.

## 2. Liquid:

The liquid used was distilled water. The column was filled with distilled water to which 4 g of commercial salt per liter was added in order to obtain a non-coalescing system. Also, few drops of pen ink were added to the liquid to make its color different from the color of bubbles to simplify the analysis of the images.

## 3. Gas:

The gas used was ambient air.

## 4. Air Pump and Plastic Tube

A small air pump with a plastic tube connecting the pump to the gas-inlet hole in the column. The pumping speed of this pump was  $0.5\text{cm}^3/\text{s}$ .

## 5. Camera:

A Mercury<sup>®</sup> 3.2Mpixel camera was used. The specifications of the camera can be seen in Appendix A.

## 6. Light Source:

A white light bulb of 500watts was used as the light source with a small lens to create a light sheet. A thin aluminum foil was put behind the column in the opposite side of the camera in order to intensify the light.

## 7. Computer:

An HP6110 Laptop was used. It has 1.4GHz processor with 256Mb of RAM. MATLAB was installed on the computer along with Adobe Photoshop 7.0 ME.

The apparatus installed is shown in Figure 4.1.

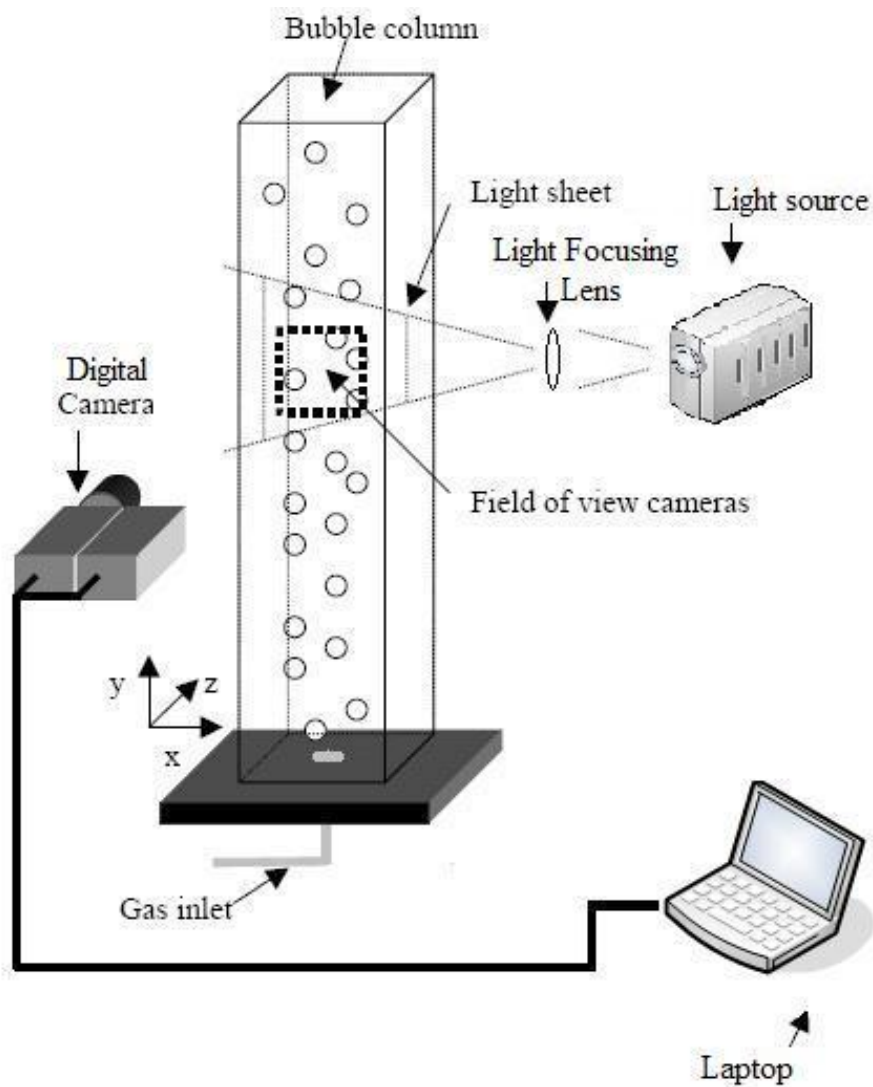


**Figure 4.1 Schematic of Experimental Setup**

### **4.3 Experimental Procedure**

1. The column was filled with distilled water to which 4 g of commercial salt (NaCl) per liter was added in order to obtain a non-coalescing system.
2. Few drops of pen ink were added to the liquid to make its color different from the color of bubbles to simplify the analysis of the images.
3. The air pump was started so as to start making bubbles inside the column.
4. The light source was turned on to provide the maximum possible visibility of bubbles.
5. Twelve images were taken using the digital camera and sent to the computer. The time between each image and the next one was 0.2 seconds. This was done three times for the three different gas inlet diameters of 0.15, 0.1, and 0.08cm

### **4.4 Computational Procedure**

1. To increase the clarity of bubbles in the chosen image, the brightness was decreased and contrast increased in order to make the liquid look darker and the bubbles look whiter. Figure 4.2 shows a sample image after the changes in brightness and contrast and Figure 4.3 shows the histogram of figure 4.2.

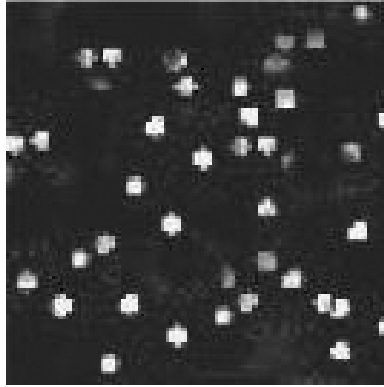


**Figure 4.2 A Sample Image of the Bubbles After Changing the Contrast and Brightness**

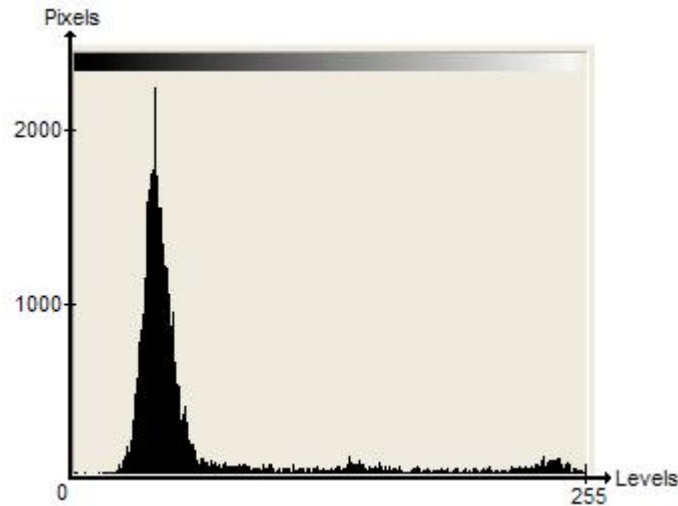


**Figure 4.3 Histogram of the Sample Image of Figure 4.2**

2. A program was created in MATLAB to read these images and analyze them to find the percentage of the bubbles in the liquid, gas hold-up. This program used the images as grayscale images and considered the gray levels 231-255 to be white (i.e. bubble) and the levels 0-230 to be black (i.e. liquid). This program can be found in Appendix B.

3. To produce another image of a single bubble to find the second parameter, one image was chosen and inverted and then a single bubble was chosen from it. And this single bubble was enlarged ten times and put into a separate image. A sample single-bubble image is shown in figure 4.4.

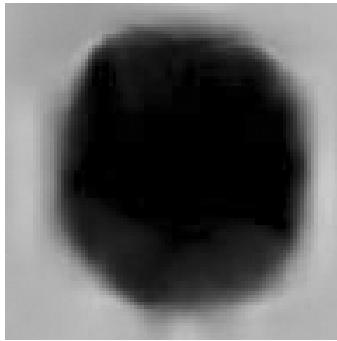


**Figure 4.4 An Inverted Image of a Single Bubble**

The single bubble was then put to scale to measure its diameter. The measurement of the diameter is crucial in checking the accuracy of the second program made in the next step.

The whole transformation process to get the single bubble image is shown in figure 4.5.

4. Another MATLAB program was created to process the single-bubble image and find the interfacial surface area of that single bubble and calculate the bubble diameter. This program can be seen in Appendix C.

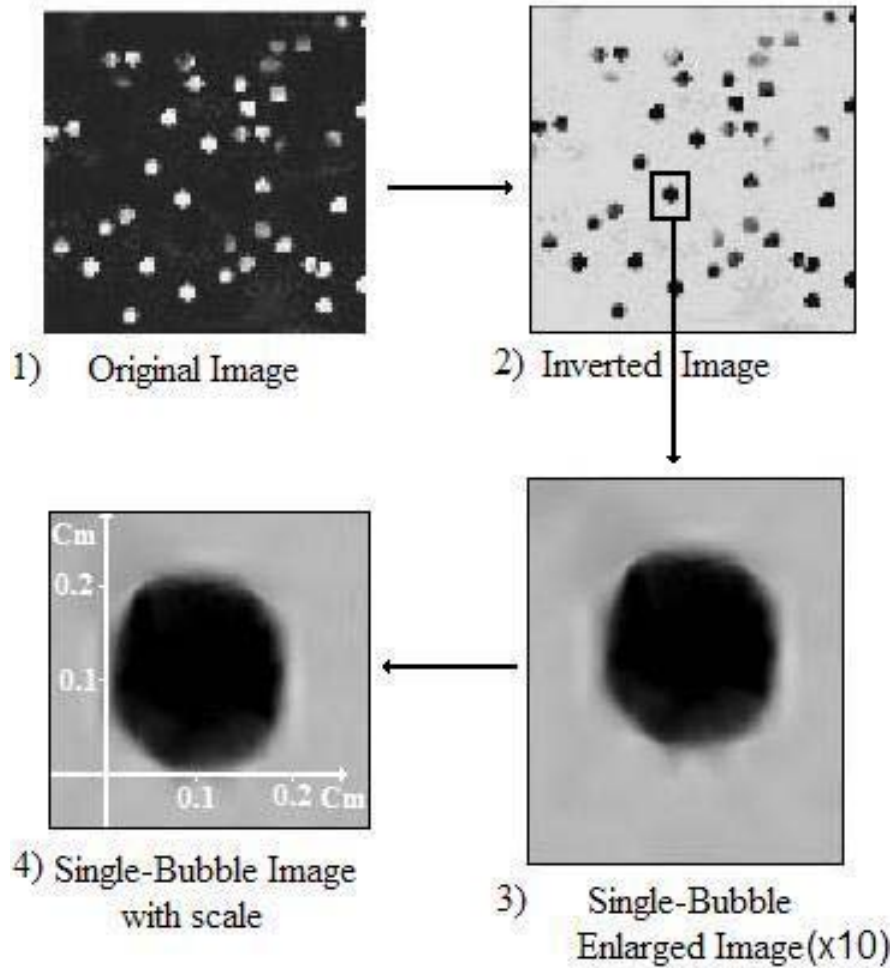


**Figure 4.5 The Process of Extracting a Single-Bubble Image from the Original Image**

And to analyze the thickness of the interfacial area and the diameter of the bubble, only level 0 was considered inside the bubble and levels 1-80 were considered the interfacial area, while levels higher than 80 were considered outside the bubble.

This procedure was repeated three times for the three different gas inlet diameters.

## **4.5 Simplifying Assumptions**

Two assumptions were made while creating the two programs. These assumptions were made to simplify the model into consideration and to simplify the calculations that need to be made to achieve the thesis aim.

These two assumptions are:

1. All bubbles are assumed to be spherical and of equal size.
2. The area instead of the size was used to find the percentage of gas bubbles in the liquid.

## **4.6 Results**

Three sets of results were produced for three different diameters of the gas inlet. As it might be clear, the gas inlet diameter has large effect on the bubble size and consequently on the gas hold-up and interfacial area. Figure 4.6 shows the 12 images taken for the gas inlet of diameter 0.15cm.

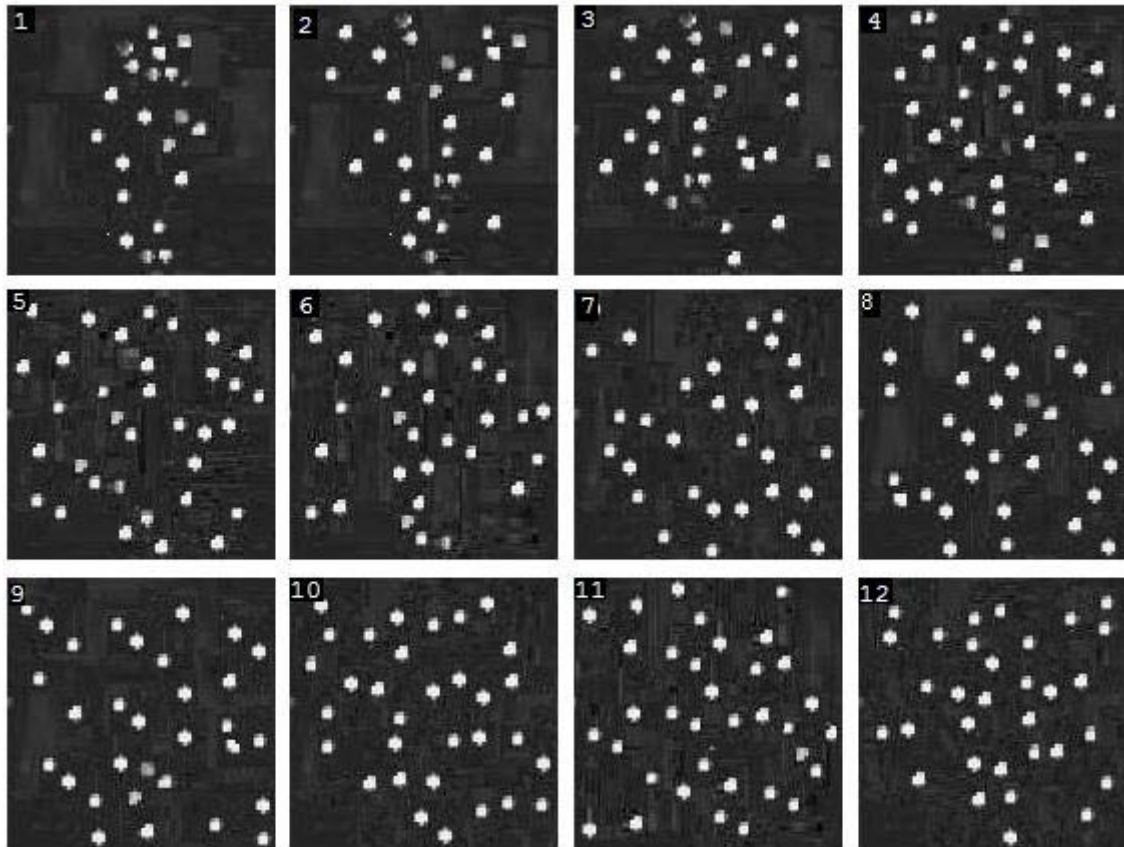


**Figure 4.6 Images of Bubbles for Gas Inlet of Diameter 0.15cm**

As a sample, figure 4.7 shows the result of running the first program on image number 8 taken for gas inlet of diameter 0.15cm. From this figure, it can be concluded that the percentage of bubbles area to the whole sample area was %1.57. The bubbles image dimensions were (134x135) pixels. And the unit for b and c in the figure is “pixel”.

```
ans =  
Number of white pixels  
  
b =  
    284  
  
ans =  
Number of non-white pixels  
  
c =  
    17806  
  
ans =  
Percentage of Bubbles area/The whole area  
  
d =  
    1.5700%
```

**Figure 4.7 The Result of Running the First Program**

The quality of the images taken was 72 pixels/inch. The result shown above is for one of the images taken. The gas hold-up of all of the 12 images taken was calculated using the program and put into a table for three different inlet diameters shown in tables 4.1.

**Table 4.1 Measured Gas Hold-up for Different Gas Inlet Diameters**

<b>Image Number</b>	<b><math>\varepsilon_G</math> for Gas Inlet of 0.15cm (%)</b>	<b><math>\varepsilon_G</math> for Gas Inlet of 0.10cm (%)</b>	<b><math>\varepsilon_G</math> for Gas Inlet of 0.08cm (%)</b>
<i>1</i>	0.6500	0.9600	1.2000
<i>2</i>	0.8500	1.1500	1.4100
<i>3</i>	1.0200	1.3200	1.5700
<i>4</i>	1.1800	1.4900	1.7400
<i>5</i>	1.3300	1.6400	1.8800
<i>6</i>	1.4600	1.7600	2.0200
<i>7</i>	1.5700	1.8700	2.1200
<i>8</i>	1.6700	1.9800	2.2200
<i>9</i>	1.7500	2.0500	2.3100
<i>10</i>	1.8200	2.1200	2.3700
<i>11</i>	1.8300	2.1200	2.3800
<i>12</i>	1.8400	2.1300	2.3800

Figure 4.8 shows a sample the result of running the second program on one bubble chosen from the 0.15cm gas inlet diameter images. From this figure, it can be concluded that the Interfacial area of the single bubble selected for the test is  $0.13709\text{cm}^2$ . The units for  $d$  and  $f$  in the figure are “cm”, and “ $\text{cm}^2$ ” respectively.

```
ans =  
Diameter of bubble  
  
d =  
    0.2100  
  
ans =  
Interfacial Area  
  
f =  
    0.1385
```

**Figure 4.8 The Result of Running the Second Program on a Sample Bubble Taken From the 0.15cm Gas Inlet Diameter Images**

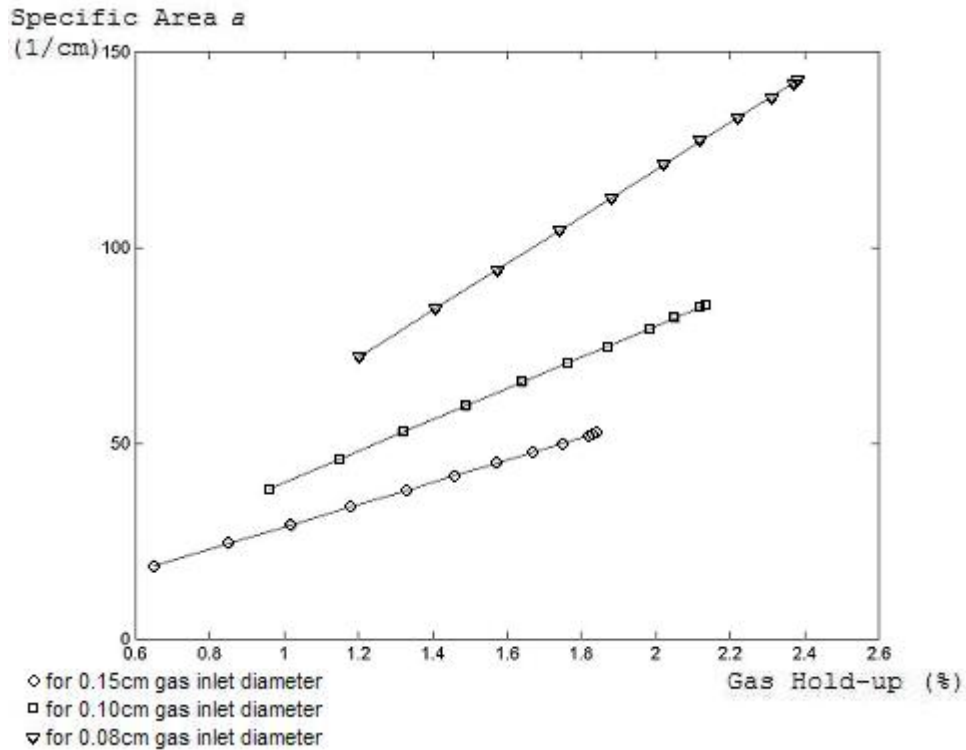
The average diameters of bubble for the gas inlet diameters of 0.15, 0.1, and 0.08cm were 0.21, 0.15, and 0.1cm, respectively.

Using equation (2.21), the specific gas-liquid interface areas were calculated for the three different diameters of gas inlet. The result of this calculation is shown in table 4.2.

**Table 4.2 Specific Gas-Liquid Interface Area for Different Diameters of Gas Inlet**

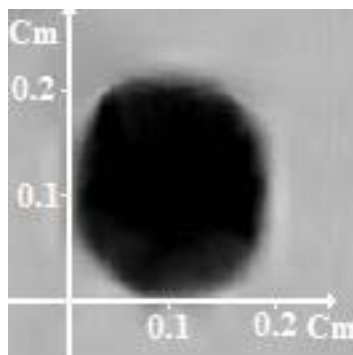
<b>Image Number</b>	<b><i>a</i> for Gas Inlet Diameter of 0.15cm (cm<sup>-1</sup>)</b>	<b><i>a</i> for Gas Inlet Diameter of 0.10cm (cm<sup>-1</sup>)</b>	<b><i>a</i> for Gas Inlet Diameter of 0.08cm (cm<sup>-1</sup>)</b>
<i>1</i>	18.5714	38.4000	72.0000
<i>2</i>	24.2857	46.0000	84.6000
<i>3</i>	29.1429	52.8000	94.2000
<i>4</i>	33.7143	59.6000	104.4000
<i>5</i>	38.0000	65.6000	112.8000
<i>6</i>	41.7143	70.4000	121.2000
<i>7</i>	44.8571	74.8000	127.2000
<i>8</i>	47.7143	79.2000	133.2000
<i>9</i>	50.0000	82.0000	138.6000
<i>10</i>	52.0000	84.8000	142.2000
<i>11</i>	52.2857	84.8000	142.8000
<i>12</i>	52.5714	85.2000	142.8000

Figure 4.9 shows the change in specific gas-liquid interface area with the change of gas hold-up for the three different diameters of gas inlet.



**Figure 4.9 Specific Area Change with Gas Hold-up Change for the Three Gas Inlet Diameters**

Figures 4.10, 4.11, and 4.12 show a single bubble extracted from images for the three different gas inlet sizes.



**Figure 4.10 A Single Bubble Produced by the 0.15cm Gas Inlet**

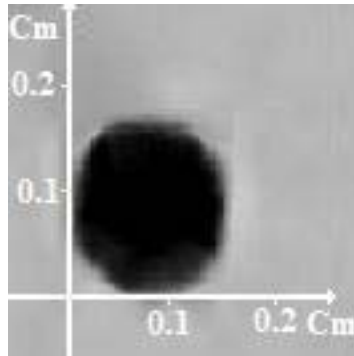


**Figure 4.11 A Single Bubble Produced by the 0.1cm Gas Inlet**

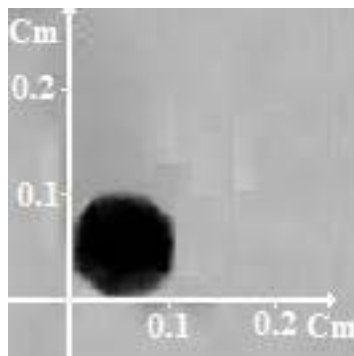


**Figure 4.12 A Single Bubble Produced by the 0.08cm Gas Inlet**

From images show in figures 4.10, 4.11, and 4.12, the thickness of interface ( $\delta$ ) was calculated. The thickness was calculated through the measurement of the number of pixels that lay in the gray levels range of 1-80 on from inside the bubble to the outside. The result of this calculation is shown in table 4.3.

**Table 4.3 Thickness of Interface and Interface Area of Bubbles for Different Gas Inlet Diameters**

Gas Inlet Diameter (cm)	Bubble Diameter $d_b$ (cm)	Bubble Interfacial Area (cm <sup>2</sup> )	Thickness of Interface, $\delta$ (cm)
0.15	0.21	0.13854015	0.00694
0.10	0.15	0.07068375	0.01046
0.08	0.1	0.031415	0.01388

Using the calculated interface thickness and the equations derived from equation (2.11),  $k_L$  values for the three different gas inlet diameters were calculated. Table 4.4 shows those calculated  $k_L$  values.

**Table 4.4  $k_L$  values for Different Gas Inlet Diameters**

Image Number	$k_L$ for Gas Inlet Diameter of 0.15cm (m/s)	$k_L$ for Gas Inlet Diameter of 0.10cm (m/s)	$k_L$ for Gas Inlet Diameter of 0.08cm (m/s)
1	0.0412	0.0300	0.0219
2	0.0429	0.0319	0.0232
3	0.0434	0.0321	0.0240
4	0.0438	0.0328	0.0246
5	0.0441	0.0331	0.0252
6	0.0444	0.0332	0.0252
7	0.0449	0.0337	0.0256
8	0.0452	0.0341	0.0260
9	0.0458	0.0345	0.0264
10	0.0460	0.0348	0.0267
11	0.0466	0.0351	0.0271
12	0.0469	0.0353	0.0272

Figure 4.13 shows the relationship between the gas hold-up and  $k_L$  values for all the three gas inlet diameters.

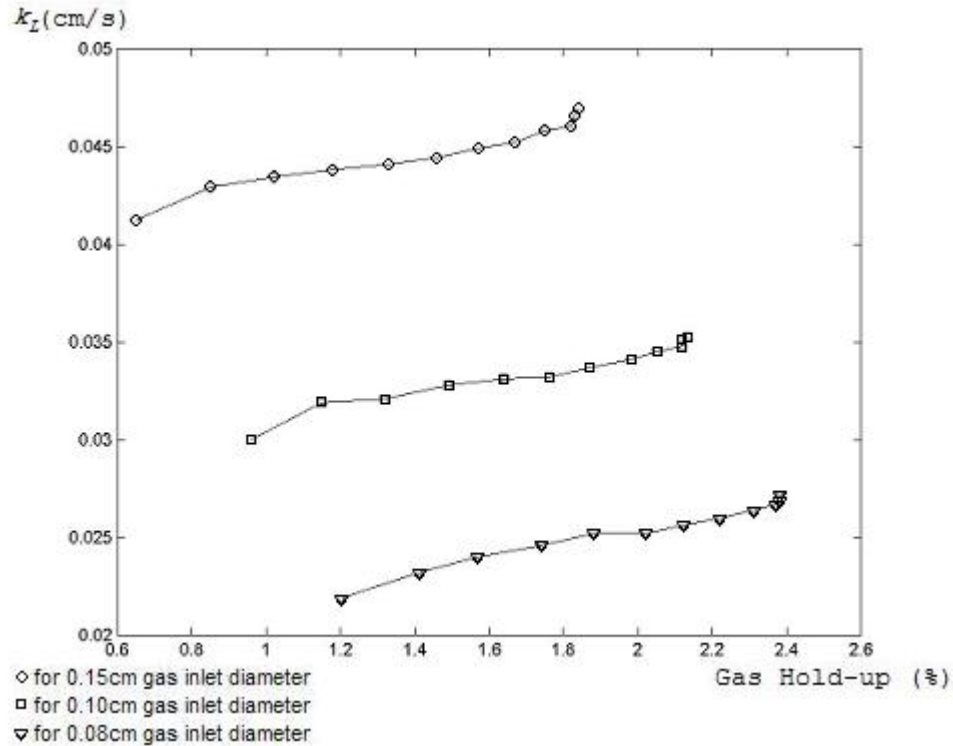


**Figure 4.13 Relation of  $k_L$  and Gas Hold-up for the Three Gas Inlet Diameters**

As  $k_L$  and  $a$  were calculated,  $k_L a$  can be calculated easily by multiplying them. The result of this multiplication was put into Table 4.5.

**Table 4.5  $k_L$ ,  $a$ , and  $k_La$  values for different Gas Inlet Diameters**

Image No.	Gas Inlet Diameter 0.15cm			Gas Inlet Diameter 0.10cm			Gas Inlet Diameter 0.08cm		
	$k_L$ (cm/s)	$a$ (1/cm)	$k_La$ (1/s)	$k_L$ (cm/s)	$a$ (1/cm)	$k_La$ (1/s)	$k_L$ (cm/s)	$a$ (1/cm)	$k_La$ (1/s)
1	0.0412	18.57	0.7653	0.0300	38.40	1.1520	0.0219	72.00	1.5768
2	0.0429	24.28	1.0421	0.0319	46.00	1.4674	0.0232	84.60	1.9627
3	0.0434	29.14	1.2660	0.0321	52.80	1.6949	0.0240	94.20	2.2608
4	0.0438	33.71	1.4774	0.0328	59.60	1.9549	0.0246	104.40	2.5682
5	0.0441	38.00	1.6754	0.0331	65.60	2.1714	0.0252	112.80	2.8426
6	0.0444	41.71	1.8534	0.0332	70.40	2.3373	0.0252	121.20	3.0542
7	0.0449	44.85	2.0141	0.0337	74.80	2.5208	0.0256	127.20	3.2563
8	0.0452	47.71	2.1572	0.0341	79.20	2.7007	0.0260	133.20	3.4632
9	0.0458	50.00	2.2915	0.0345	82.00	2.8290	0.0264	138.60	3.6590
10	0.0460	52.00	2.3930	0.0348	84.80	2.9510	0.0267	142.20	3.7967
11	0.0466	52.28	2.4365	0.0351	84.80	2.9765	0.0271	142.80	3.8699
12	0.0469	52.57	2.4677	0.0353	85.20	3.0076	0.0272	142.80	3.8842

Figure 4.14 shows the relationship between  $k_La$  and the gas hold-up for the three different gas inlet diameters.

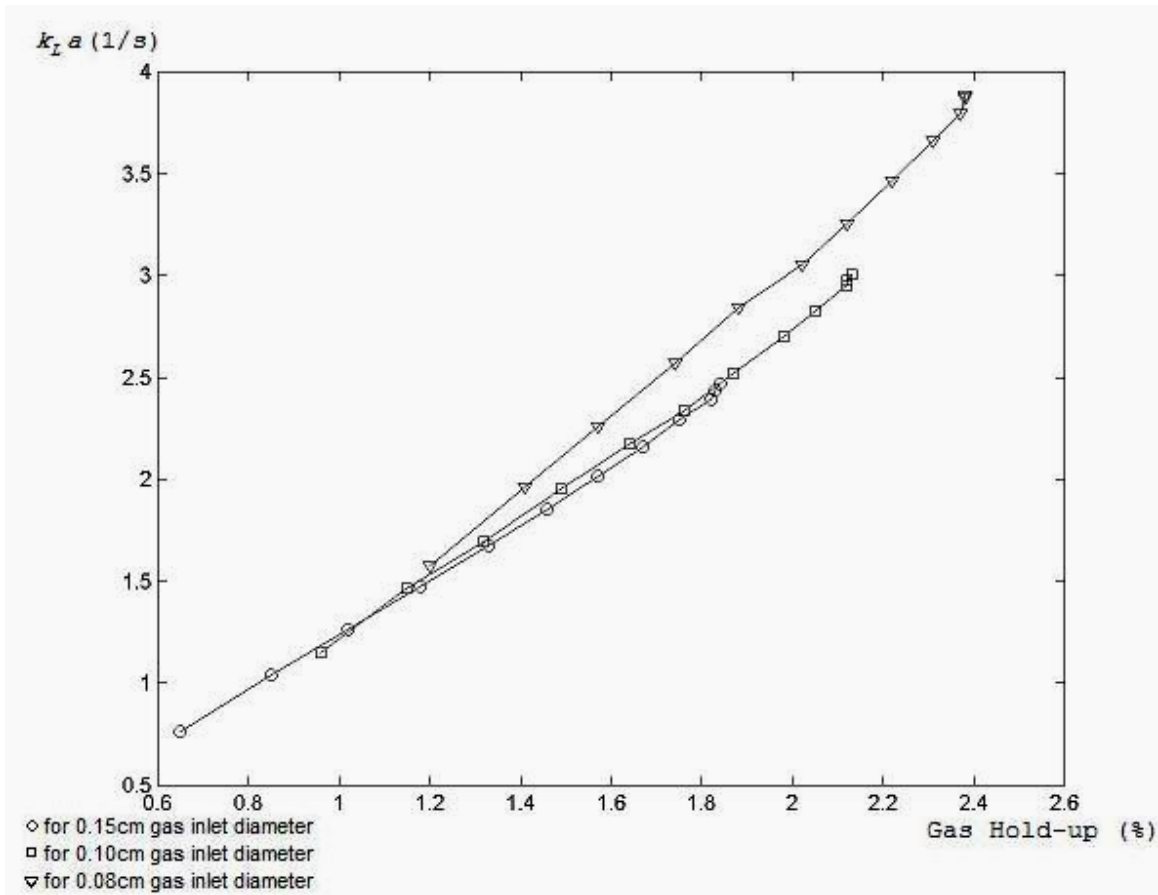


**Figure 4.14 Relation of  $k_L a$  and Gas Hold-up for the Three Gas Inlet Diameters**

#### 4.7 Discussions

A first step of checking the accuracy of the system was to calculate the gas hold-up for the three different gas inlet diameters. The calculated  $\varepsilon_G$  was compared to the experimental result in figures 4.15, 4.16, and 4.17 for each of the gas inlet diameters.

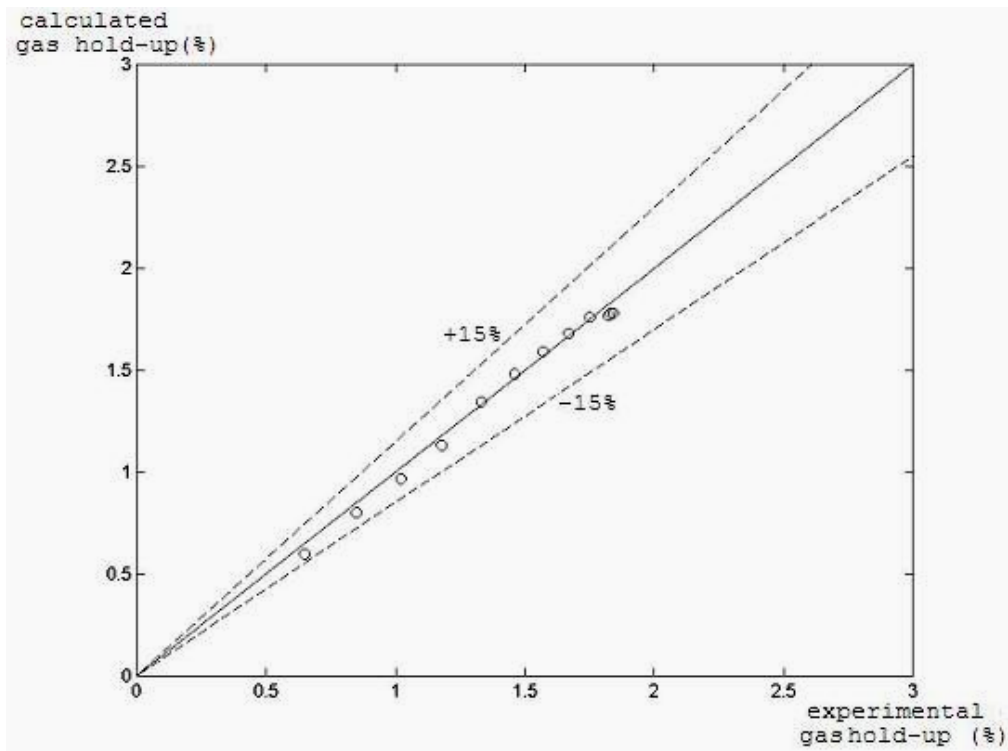


**Figure 4.15 Experimental and Calculated Values of  $\varepsilon_G$  for Gas Inlet Diameter of 0.15cm**

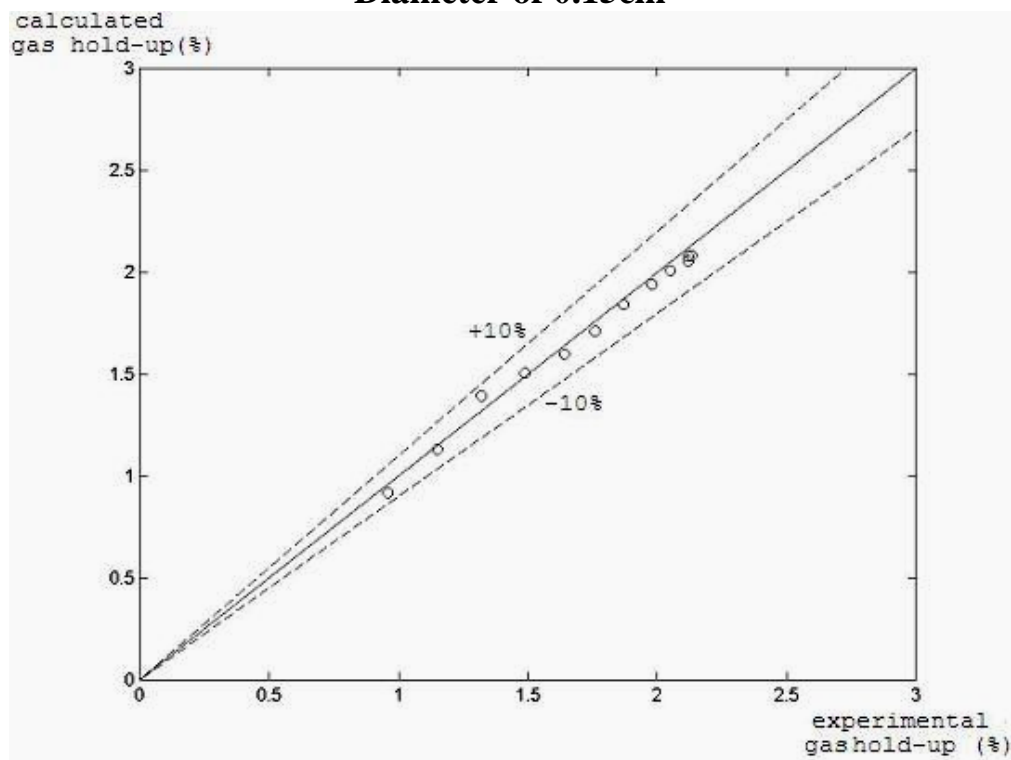


**Figure 4.16 Experimental and Calculated Values of  $\varepsilon_G$  for Gas Inlet Diameter of 0.10cm**

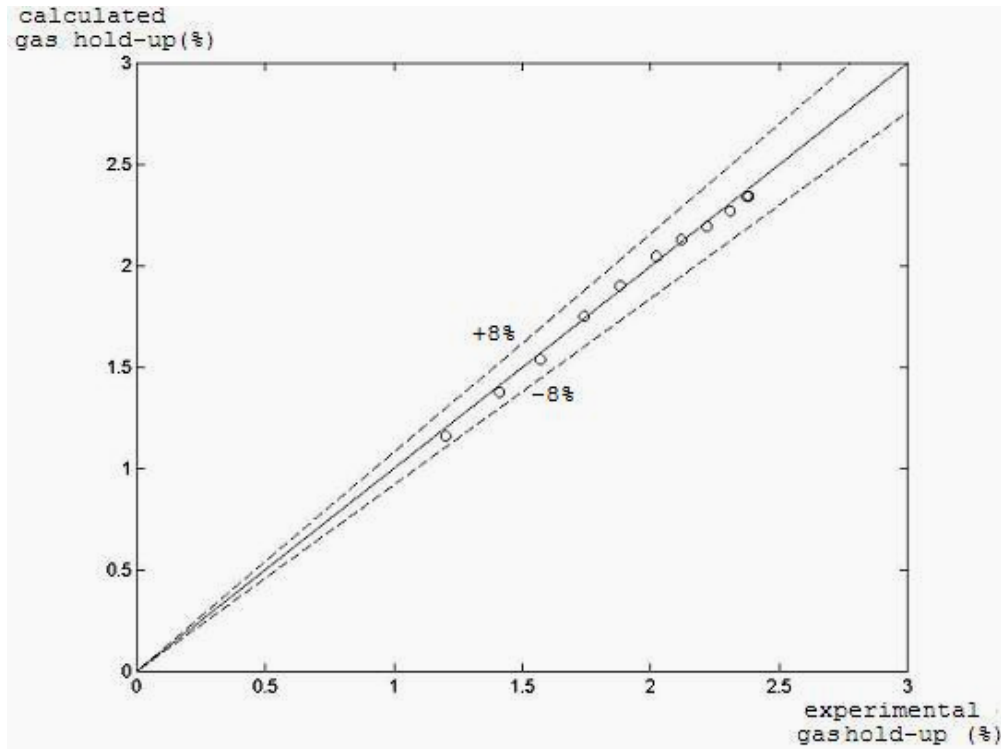


**Figure 4.17 Experimental and Calculated Values of  $\epsilon_G$  for Gas Inlet Diameter of 0.08cm**

Figures 4.15, 4.16, and 4.17 show that the error of measuring  $\epsilon_G$  is  $\pm 8-15\%$ .

This error rate tends to be acceptable as compared to a  $\pm 30\%$  reported by a similar experiment done by Vasconcelosa, J. M. T., Rodrigues, J. M. L., Orvalho, S. C. P., Alves, S. S., and Mendesb, R. L., Reis, A. [29].

To evaluate the accuracy of the second program in calculating the interfacial surface area, this area was calculated manually for this chosen test bubble. The manually calculated results were obtained from calculating the diameter of the bubble by number of pixels and convert it into centimeters, as the image resolution was 72 pixel/inch.

And the result was compared to the one obtained from the second program.

This simple comparison can be seen in table 4.6.

**Table 4.6 Comparison of Manually Obtained Results and Results of Program 2**

Result Source	Gas Inlet Diameter 0.15cm		Gas Inlet Diameter 0.10cm		Gas Inlet Diameter 0.08cm	
	Bubble Diameter (cm)	Interfacial Surface Area (cm <sup>2</sup> )	Bubble Diameter (cm)	Interfacial Surface Area (cm <sup>2</sup> )	Bubble Diameter (cm)	Interfacial Surface Area (cm <sup>2</sup> )
Calculated Result	0.2097	0.1381	0.1511	0.0717	0.0996	0.0311
Program 2 Result	0.2100	0.1385	0.1500	0.0706	0.1000	0.0314

From table 4.6, it can be seen that the accuracy of the second program is high and the error was about 0.9% in the worst case, which is acceptable.

Another step was done to assure the accuracy of the results obtained.

Another comparison was made with results obtained from a similar experiment measuring the hydrodynamics of gas-liquid mass transfer between oxygen and water Vasconcelosa, J. M. T., Rodriguesa, J. M. L., Orvalho, S. C. P., Alves, S. S., and Mendesb, R. L., Reis, A. [29]. The values of  $k_La$  obtained were put in a graph along with the ones obtained from reference [29] in order to measure the discrepancies between them. This can be seen in figure 4.18.

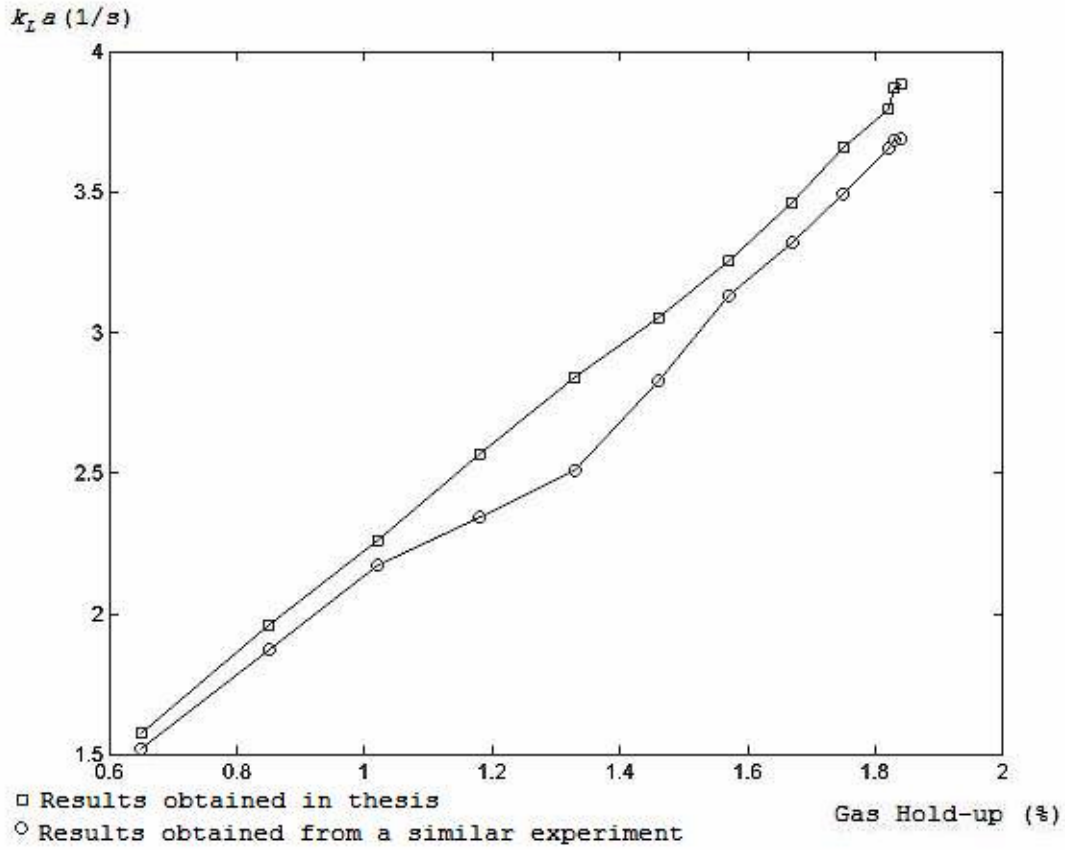


**Figure 4.18 Comparison of  $k_L a$  Obtained in Thesis and  $k_L a$  from a Similar Experiment**

The comparison was made between the  $k_L a$  values for the gas inlet of diameter 0.08cm, as it is the closest to the environment of the experiment mentioned in Vasconcelosa, J. M. T., Rodriguesa, J. M. L., Orvalho, S. C. P., Alves, S. S., and Mendesb, R. L., Reis, A. [29].

The showing differences are due to the simplifying assumptions made in section 4.5. Assuming that all bubbles are of the same size gives a minor difference in measuring the gas hold-up, and that difference builds up when doing more dependant calculations.

The parameters calculated using the results extracted from the taken images show that these results comply with the expected values of  $k_L$  and  $k_L a$  mentioned in reference Kaskiala, T., [18] from section 2.3.2.

The results obtained from the two programs can be used in studying the hydrodynamics of the bubble column reactors. The two obtained parameters, gas hold-up and interfacial surface area, can be used to provide more understanding of the behavior of mass-transfer in gas-liquid systems. In the results section of this chapter, it has been shown that many other hydrodynamic parameters can be obtained from the images used and the results extracted from them like  $k_L$ ,  $a$ , and  $k_L a$ .

Furthermore, the same system can be used to obtain the same parameters for stirred tank models as well as for bubble column.

One thing to put in mind is that all the apparatus used in this experiment is simple, cheap, and accurate equipments. This is an important issue in measuring the usability and applicability of the solution provided.

The provided system can also be used to obtain information about almost any kind of gas-liquid combination used in a bubble column reactor. The two parameters extracted from the image are important in studying the hydrodynamics of bubble columns. The only two things that will need to be

changed in the programs are the values of the variables N and M, which are the dimensions of the image used in the calculations.

Other results can also be obtained by using more apparatus. For example, an electrode can be used to measure the concentration of oxygen in the water and in the atmosphere. This would result in the value of  $\Delta C$ , thus, the calculation of the mass transfer rate using the equation (2.11).

One last note to be said about the system is that the computer software used to obtain these results, MATLAB and Adobe Photoshop 7.0 ME, is widely used and is not expensive as compared to other image processing software packages.

## ***CHAPTER FIVE***

### ***CONCLUSIONS AND FUTURE WORK***

#### **5.1 Conclusions**

From the experimental and computational parts of this thesis, the following points were concluded:

1. A computerized system was created to measure the percentage of gas bubble in a liquid and measure the interfacial surface area of a single bubble.
2. The system created used simple, inexpensive, yet accurate apparatus.
3. The suggested system was tested and has proved good accuracy.
4. The same apparatus and installation can be used to measure the two parameters measured for any gas-liquid bubbly flow. The only two things that will need to be changed in the programs are the values of the variables N and M, which are the dimensions of the image used in the calculations in pixels.
5. This system can be used also for stirred tank models, not only for bubble columns, without changing anything in the apparatus or procedure.

6. The accuracy of the second program devoted to finding the interfacial surface area was evaluated by comparing the results obtained with ones calculated manually. The error percentage for this program was 0.9%.
7. The programs were created using MATLAB which is a widely used engineering software. And the image manipulations were done using Adobe Photoshop 7.0 ME which is also commonly used image manipulation software.

## **5.2 Suggestions for Future Work**

As a continuation of this work, few steps can be made in the following directions:

1. Other programs can be created to extract more parameters from the images obtained such as the bubble velocity.
2. The same system can be used to obtain information on other types of gases and liquids and on stirred tank models.
3. More accurate camera can be used to obtain higher quality in images. This would lead to higher accuracy in the computations.
4. The same system can provide higher accuracy in measurements if a shorter time interval was applied between the photos.

## REFERENCES

- [1] Tatterson, G. B., *Fluid Mixing and Gas dispersion in agitated tanks*. McGraw-Hill, 1991.
- [2] Akita, K., Yoshida, F., “*Bubble size, interfacial area, and liquid phase mass transfer coefficient in bubble columns*”, *Ind. Eng. Chem., Process Des. Dev.* 13, No. 4. Pages 84-91, 1974.
- [3] Fukuma M., Muroyama K., Yasunishi A., “*Specific gas-liquid interfacial area and liquid-phase mass transfer coefficient in a slurry bubble column*”, *Japan Chem Eng. Journal*, Vol. 20, No. 3, Pages 321-324, 1987.
- [4] Adrian, R. J., “*Particle-imaging techniques for experimental fluid mechanics*”, *Ann. Rev. Fluid Mechanics* 22, Pages 261–304, 1991.
- [5] Becker, S., Sokolichin, A. & Eigenberger, G., “*Gas-liquid flow in bubble columns and loop reactors: Part II. Comparison of detailed experiments and flow simulations*”, *Chem. Eng. Sci.* 49, Pages 5747–5762, 1994.
- [6] Broder, D. & Sommerfeld, M., “*A PIV/PTV system for analyzing turbulent bubbly flows*”, In *Proceedings of 10th Int. Symp. on Appl. of Laser Techniques to Fluid Mech.*. Lisbon, Portugal, 2000.
- [7] Deen, N. G., Hjertager, B. H. & Solberg, T., “*Comparison of PIV and LDA measurement methods applied to the gas-liquid flow in a bubble*

*column*”, In Proceedings of 10th Int. Symp. on Appl. of Laser Techniques to Fluid Mech.. Lisbon, Portugal, 2000.

[8] Deen, N. G., “*An Experimental and Computational Study of Fluid Dynamics in Gas-Liquid Chemical Reactors*”, PhD. Thesis, Department of Chemistry and Applied Engineering Science Aalborg University Esbjerg, Denmark, 2001.

[9] Lain, S., Broder, D. & Sommerfeld, M., “*Numerical simulations of the hydrodynamics in a bubble column: quantitative comparisons with experiments*”, In Fourth Int. Conf. On Multiphase Flow, ICMF-2001. New Orleans, USA, 2001.

[10] Grau R. A., and Heiskanen K., “*Visual technique for measuring bubble size in flotation machines*”, Min. Engineering Journal, No. 15, Pages 507-513, 2002.

[11] Merchuk J.C., “*Basic Models for Mass Transfer: Modular Instruction Series, module B4.4*”, AIChEMI Modular Instruction, Series B, Pages 33-38, 1983.

[12] Cussler E.L., *Diffusion, Mass transfer in fluid systems*, 2<sup>nd</sup> ed., Cambridge University Press, UK, 1997.

[13] Danckwerts P.W., “*Significance of liquid-film coefficients in as absorption*”, Ind. Eng. Chem., No 43, Pages 1460-1467, 1951.

- [14] Whitman W.G., “*Preliminary experimental confirmation of two-film theory of gas absorption*”, Chem. Metall. Eng., Vol. 29, No. 251, Pages 146-149, 1923.
- [15] Moo-Young M., Blanch H.W., *Design of biochemical reactors, Mass transfer criteria for simple and complex systems*, Pages 746-753, 1987.
- [16] Higbie R., “*The rate of absorption of a pure gas into a still liquid during short periods of exposure*”, Trans. Am. Inst. Chem. Eng., No. 35, Pages 36-60, 1935.
- [17] Toor H.L., Marchello J.M., “*Film-penetration model for mass transfer and heat transfer*”, Am. Inst. Chem. Eng. Journal, No. 4, Pages 97-101, 1958.
- [18] Kaskiala T., “*Studies On Gas-Liquid Mass Transfer In Atmospheric Leaching Of Sulphidic Zinc Concentrates*”, Doctoral Thesis, Helsinki University of Technology, 2005.
- [19] Van't Riet K., “*Review of measuring methods and results in nonviscous gas-liquid mass transfer in stirred vessels*”, Ind. Eng. Chem. Process Des. Dev., Vol. 18, No. 3, Pages 357-364, 1979.
- [20] Wilkinson P. M., Haringa H., Van Dierendonck L.L., “*Mass transfer and bubble size in bubble column under pressure*”, Chem. Eng. Sci., Vol. 49, No. 9, Pages 1417-1427, 1994.

- [21] Zhu Y., Wu J., “Gass-to-liquid mass transfer in hot sparged system”, Proceedings, 9<sup>th</sup> APCCChE 2002 and Chemeca 2002, Christchurch, New Zealand.
- [22] Yang W., Wang J., Jin J., “*Gas-Liquid Mass transfer in slurry bubble column reactor under high temperature and high pressure*”, Chinese Journal of Chemical Eng., Vol. 9, No. 3, Pages 253-257, 2001.
- [23] Rautio M., “*Gas-Liquid Mass Transfer*”, Master’s thesis, Helsinki University of Technology, Finland, 1996.
- [24] Sada E., Kumazawa H., Lee L.H., Iguchi T., Ing. Eng. Chem. Precess Des. Dev., Vol. 25, No. 2, Pages 472-476, 1986.
- [25] O’Conner C.T., Randall E.W., Goodall C.M., “*Measurement of the effect of physical and chemical variables on bubble size*”, Int. Journal of Mineral Processing, No. 28, Pages 139-149, 1990.
- [26] Fogg P.G.T., Gerard W., *Solubility of gases in liquids*, Chishester, UK, 1991.
- [27] Van Sint Annaland M., Dijkhuizen W., Deen N. G., and Kuipers J. A. M., “*Numerical Simulation of Behavior of Gas Bubbles Using a 3-D Front-Tracking Method*”, Published online September 12, 2005 in Wiley InterScience ([www.interscience.wiley.com](http://www.interscience.wiley.com)).

- [28] Darmana D., Deen N.G., Kuipers J. A. M., “*Detailed 3D Modeling of Mass Transfer Processes in Two-Phase Flows with Dynamic Interfaces*”, Chem. Eng. Technol. 2006, 29, No. 9, Pages 1027–1033, 2006.
- [29] Vasconcelosa J. M. T., Rodriguesa J. M. L., Orvalho S. C. P., Alves S. S., and Mendesb R. L., Reis A., “*Effect of contaminants on mass transfer coefficients in bubble column and airlift contactors*”, Chemical Engineering Science 58, Pages 1431 – 1440 , 2003.

**APPENDIX A**  
**THE SPECIFICATIONS OF THE CAMERA USED IN THE**  
**EXPERIMENT**

---

**Specifications**

Sensor	3.2 megapixel CMOS
Lens	F 2.8 ~ 8.47
Built-In Viewfinder	Field of View: 85%
Focus Range	Normal: 100 cm ~ infinity Macro: (W) 20cm
Sensitivity	Auto, 100, 200, 400
LCD Display	1.5" color TFT LCD panel
Still Image Resolution	2272x1704, 2048x1536, 1024x768
Video Resolution	320x240
Still Image Quality	Fine: 7X compression rate Normal: 10X compression rate
Exposure Meter	Center-weighted average, Multi-pattern TTL AE
Exposure Control	Auto & manual
Exposure Compensation	-2EV to +2EV (-2.0, -1.7, -1.3, -1.0, -0.7, -0.3, 0.0, +0.3, +0.7, +1.0, +1.3, +1.7, +2.0)
Shutter Control	Mechanical shutter, shutter speed: 1/2-1/6458 sec. With CCD variable electronic shutter
Digital Zoom	Preview Mode: up to 4X Playback Mode: up to 4X
Image File Format	EXIF 2.1 compatible format (JPEG compression) DCF compatible. Supports DPOF
White Balance	Auto/Manual (4 modes in manual selection: daylight/ shade/ tungsten/fluorescent)
Picture Storage	Internal: 16 MB embedded Nandgate flash memory External: SD memory card/MMC
Microphone	Built-In
Sound Feedback	Speaker
Communication Interface	USB 1.1
Self-Timer	2 steps, 2-10 sec. with beep sound
Playback Mode	Single/9 thumbnails
TV System	NTSC/PAL selectable
Power Supply	AAA-size alkaline batteries x 4 Rechargeable Ni-MH batteries (min. 550 mAh / 1.2 V)
Dimensions	Camera body: 97 x 28 x 63 mm
Weight	Camera body without battery: 110g

\* Specifications are subject to change without notice.

## ***APPENDIX B***

### ***MATLAB PROGRAM TO CALCULATE THE PERCENTAGE OF BUBBLES IN THE LIQUID***

```
a = imread ('bubbles','jpg');
info = imfinfo('bubbles','jpg');
N = 134;
M = 135;
b=0;
c=0;
for i= 1:M,
    for j=1:N,
        if a(i,j) > 230
            b=b+1;
        else
            c=c+1;
        end
    end
end
'Number of white pixels'
b
'Number of non-white pixels'
c
'Percentage of Bubbles area/The whole area'
d=(b/(N*M))*100
```

## *APPENDIX C*

### *MATLAB PROGRAM TO CALCULATE THE INTERFACIAL SURFACE AREA OF ONE BUBBLE*

```
a = imread ('lbub', 'jpg');
N = 97;
M = 97;
c=0;largest=0;d = 0.0;
for i= 1:M,
    b=0;
    for j=1:N,
        if a(i,j) == 0
            b=b+1;
        end
    end
    if b > largest
        c = i;
        largest = b;
    end
end
'The line with the most black pixels'
c
'Number of pixels'
largest
'Diameter of bubble'
d=(largest/720)*2.5
'Interfacial Area'
f=d*d*3.1415
```

## الخلاصة

هذه الأطروحة تقدم نظاماً مبسطاً لدراسة و تصميم مفاعلات عمود الفقاعة. النظام المقترح يركز على دراسة إثنين من أهم الخواص لعمليات نقل الكتلة بين الغازات و السوائل. هذه الخواص الأثنين هي نسبة الفقاعات الغازية في السائل و مساحة المنطقة السطحية التفاعلية لواحدة من الفقاعات.

تم فحص النظام المقترح بإستخدام الماء كسائل و الهواء الجوي كغاز. و الصور المأخوذة تم التلاعب بها و تحليلها من خلال برامجيات الحاسبة لأنتاج المعلومات المطلوبة. تم التلاعب بالصور من خلال برنامج ادوبي فوتو شوب الإصدار السابع و تم تحضير برنامجين بلغة برمجة مات لاب الإصدار 5.3 لغرض إستخلاص المعلومات المطلوبة من الصور.

تم تحصيل ثلاثة مجاميع مختلفة من النتائج لثلاثة أقطار مختلفة لفتحة مدخل الغاز الأولى لقطر 0.15 سم و الثانية لقطر 0.10 سم و الأخيرة لقطر 0.08 سم. النتائج كانت مرضية و نسبة الخطأ في قياس مساحة المنطقة السطحية التفاعلية لواحدة من الفقاعات كانت 0.9%. بينما تراوحت نسبة الخطأ في قياس نسبة الغاز الموجود في السائل بين 8% و 15%.

تراوحت قيمة نسبة الغاز الموجود في السائل المستنتجة لمدخل الغاز ذو قطر 0.15 سم بين 0.65% و 1.84%. بينما تراوحت نسبة الغاز الموجود في السائل لمدخل الغاز ذو

قطر 0.10 سم بين 0.96% و 2.13%. و لقطر مدخل الغاز 0.08% تراوحت نسبة الغاز الموجود في السائل بين 1.2% و 2.38%.

و كان معدل قطر الفقاعة لمداخل الغاز ذات الأقطار 0.15 سم، 0.10 سم، و 0.08 سم تساوي 0.21 سم، 0.15 سم، و 0.1 سم على التوالي.

من الممكن استخدام نفس النظام في دراسة الخواص الهيدروديناميكية لنظام الخزان ذو المحرك بالإضافة إلى نظام عمود الفقاعة. وكانت المعدات المختبرية المستخدمة في هذا النظام بسيطة و رخيصة الكلفة و دقيقة بشكل مقبول.

## شكر و تقدير

من بعد شكر الله تعالى و حمده أتوجه بالثناء إلى الأستاذ المشرف الدكتور نصير الحبوبى لمجهوداته الإستثنائية التي قام بها لإيصال هذا العمل إلى بر الأمان. و أتوجه كذلك بالشكر إلى السيد رئيس قسم الهندسة الكيماوية و الكادر التدريسي و الإداري في القسم للمساعدة و الإسناد الذي قدموه لي أثناء و قبل فترة البحث.

و أتوجه بالشكر إلى عائلتي العزيزة التي صبرت و تحملت معي الظروف العصيبة التي مرت علينا لإنجاز هذا العمل.

مروة طارق

# طريقة مبنية على تحليل الصور لقياس ذوبان الغازات في السوائل و معامل إنتقال الكتلة

رسالة

مقدمة إلى كلية الهندسة في جامعة النهريين  
و هي جزء من متطلبات نيل درجة ماجستير علوم  
في الهندسة الكيمياوية

من قبل

مروة طارق رشيد

(بكالوريوس علوم في الهندسة الكيمياوية 2004)